Dynamics and Transport of Sulfur Dioxide over the Yellow Sea during TRACE-P

Fang Huang Tu, Donald C. Thornton, Alan R. Bandy, and Mi-Sug Kim

Department of Chemistry, Drexel University, Philadelphia, Pennsylvania

Gregory Carmichael and Youhua Tang

CGRER, University of Iowa, Iowa City, Iowa

Lee Thornhill and Glenn Sachse

NASA Langley Research Center, Hampton, Virginia

Abstract

Fast time resolution (>1 Hz) sulfur dioxide (SO_2) measurements were obtained using an atmospheric pressure ionization mass spectrometer with isotopically labeled internal standard on the NASA Wallops P-3B during the NASA TRACE-P field experiment. The high time resolution for SO_2 allowed a view into the dynamics of SO_2 transport, including the effects of clouds. Two missions along 124.5^{o}E from the vicinity of Taiwan to the northern Yellow Sea near the Korean peninsula were flown on consecutive days with quite different weather conditions. Although the winds on both flights were westerly to northwesterly, the SO_2 concentrations were markedly different in vertical and horizontal distributions. Together with turbulence measurements and other high rate data on the P-3B, we have assessed how cloud processing and atmospheric dynamics may have caused the differences in the SO_2 distributions. Below 2 km SO_2 layers of a few hundred meters depth were often isolated from the mixed layer. The relatively slow process of entrainment limited loss of SO_2 to the marine mixed layer. When compared to 3-D model results of

SO_2 along the flight track, the *in situ* SO_2 data showed that the model poorly represented the SO_2 distribution along the flight track for the cloudy day while the model gave a reasonably good representation of the *in situ* data during the clear air flight. On the clear air flight day, the model achieved a closer representation of the SO_2 distribution, but it overestimated the SO_2 concentrations just above the well-mixed boundary layer. The deviations between the observations and the model appear to be related the treatment of the boundary layer dynamics.

1. Introduction

The high level of economic development in east Asia during the past two decades has relied on fossil fuels for energy production, in particular, on high sulfur content coal. Sulfur dioxide (SO_2) emissions peaked in 1996 in the major source regions of East Asia, but the total emissions of SO_2 are still very large [*Streets et al.*, this issue]. The NASA Global Troposphere Experiment (GTE) TRAnsport and Chemical Evolution over the Pacific (TRACE-P) mission was designed to study the transport and evolution of anthropogenic chemical species and their impact on the north Pacific troposphere [*Jacob et al.*, this issue]. The TRACE-P mission employed a wider suite of measurements than in past GTE missions and a wide variety of predictive chemical and meteorlogical models than earlier field programs in this region.

Sulfur dioxide plays a very important role in atmospheric sulfur cycle through its role in the formation of new aerosol and the modification of existing aerosol. The major sources of SO_2 are from anthropogenic fuel combustion and from volcanoes. The reliance of East Asian nations on fossil fuels in their rapid development over the last two decades has lead to concern about the potential impact of SO_2 on the western Pacific troposphere. There is also the concern about the impact on global climate through the formation and modification of aerosols and their effects on

the radiation balance of the atmosphere. Assessing the relative contributions of anthropogenic and volcanic sources can be done through estimates of the anthropogenic emissions and the flux of SO_2 from volcano emissions. Neither of these estimates is easy to determine precisely because the large area over which the anthropogenic sources are dispersed and the remoteness and difficulty in measuring the SO_2 fluxes from volcanoes.

The NASA Pacific Exploratory Missions West (PEM West) studied the western Pacific region in September 1991 (phase A) [*Hoell et al.*, 1996] and in February – March 1994 (phase B) [*Hoell et al.*, 1997]. The anthropogenic SO_2 measurements from these earlier missions [*Thornton et al.*, 1996, 1997] have clearly shown the impact on the northern Pacific when compared to the central and southern Pacific [*Thornton et al.*, 1999]. Volcanic sources of SO_2 have also been a significant source of SO_2 to the Pacific troposphere, and they remain a significant source in this region, particularly around Japan [*Venkze et al.*, 2002]. Transport of 0.1-2 ppbv of SO_2 over the Yellow Sea in mid to late April has been observed to be variable between the surface and 3 km with the highest concentrations below 1 km [*Kim et al.*, 2001]. How SO_2 is transported from its sources and how SO_2 impacts the western Pacific troposphere are very important issues that are not fully resolved.

During the TRACE-P mission, the fast time resolution (>1Hz) SO_2 data allowed a view of the dynamics of SO_2 transport. This high time resolution allowed the study of small spatial scale features of SO_2 in and around clouds, in ship plumes, and the vertical profile in plumes. With the turbulent air motion measurement system (TAMMS) [*Thornhill et al.*, this issue] on the NASA Wallops Flight Facility P-3B, we were able to study the details of the vertical distribution of SO_2 in the lower troposphere and in the marine mixed layer on the time scales of the atmospheric turbulence. The results of the TRACE-P experiment will shed new light on the role

of atmospheric dynamics in controlling the distribution of SO_2. As a consequence we can better understand how long range transport of SO_2 occurs over the northern Pacific.

2. Experiment

On the TRACE-P mission, the SO_2 measurements on the NASA Wallops P-3B were obtained by atmospheric pressure ionization mass spectrometry using an isotopically labeled internal standard (APIMS/ILS). The details of the quadrupole APIMS/ILS system with a ^{63}Ni ion source have been described recently [*Thornton et al.,* 2002a]. In short, the technique involves continuously adding $^{34}SO_2$ as an internal standard to ambient air as it is drawn into the aircraft through a Teflon lined inlet through the aircraft wall [*Bandy et al.,* 1993]. The ion chemistry and declustering region produced SO_5^- ions, which were monitored alternately at m/e 112 for the ambient signal and m/e 114 for the internal isotopically labeled standard. Each ion signal count was integrated for 20 ms and the ambient SO_2 concentration was computed for every 40 ms (25 Hz sampling rate) after taking into account the isotopic abundances as described previously [*Bandy et al.,* 1993]. A correction was also made for background ion signals determined from SO_2 free air (Scott-Marrin, Inc, Riverside, CA) and from ambient air without the standard added [*Thornton et al.,* 2002a].

The TRACE-P data archive contains a 1 second integral of 25 Hz data. The lower limit of detection for 10 sec integration is 1 pptv. The precision is estimated to be 3 pptv for a 1 sec integration for SO_2 concentrations below 100 pptv and <2% above 100 pptv. Accuracy of the measurements is estimated to be 5% based on calibration of the 153 ppbv $^{34}SO_2$ in ultrapure nitrogen cylinder (Scott-Marrin, Inc., Riverside, CA) using three $^{32}SO_2$ permeation tubes (VICI Metronics, Poulsbo, WA), which were gravimetrically calibrated.

The TAMMS provided 25 Hz data for the *u*, *v*, *w* components of the wind, water vapor mixing ratio (MR) from a Lyman α absorption sensor, static temperature, and pressure [*Thornhill et al*., this issue]. The SO_2 count data were recorded by the TAMMS data system to insure that the time recorded for the SO_2 counts would be identical to the time recorded for the three component wind data. Additional meteorological data were provided by the GTE project for the P-3B [TRACE-P data archive].

Five day backward trajectories [http://www-gte.larc.nasa.gov/trace/TP_dat.htm] were calculated using a kinematic model, i.e., employing the *u*, *v*, and *w* wind components from the ECMWF analyses [*Fuelberg et al*., this issue]. A cubic spline procedure was used to vertically interpolate the gridded data from the 61 initial sigma levels to 191 constant pressure levels at 5-hPa intervals between 1000 and 50 hPa. Linear interpolation provided values within these 5-hPa intervals and at the parcel's precise horizontal locations. Linear interpolation also was used to temporally interpolate at 5-min time steps. Additional details about the trajectory model, along with a comparison between kinematic and isentropic trajectories, are given in *Fuelberg et al.* [1996].

3. Results

One of the major goals of TRACE-P was to understand the processes that control the transport and evolution of chemical species in the Pacific troposphere. Predictive and interpretive chemical transport models are useful tools for understanding the large scale of the transport and the chemical processing that occurs over the Pacific because of the difficulty of obtaining data on a regular basis. The large scale view depends on a myriad of processes that descend into smaller and smaller scales down to the order of molecular processes. The capability of the model output

in representing actual conditions as indicated by observations depends on the quality of the estimates of the chemical inputs and the validity of the parameterizations that must be used to account for the small scale chemical and physical processes that cannot be easily represented in fine detail or where the details of the process are not completely known.

The availability of high time and spatial resolution data provides a broader base on which to evaluate model output. This more detailed database also provides an input of information with which to refine the model process parameterizations. Most transport models have very good representation of the meteorological processes that occur over small and large scales because of the volume of data that is available. The representation of chemical processes also can provide good representations of the chemical field for homogeneous gas phase chemistry. The primary uncertainties with chemical transport models appear to be on the links between the physical and chemical processes [*Chin et al.*, 2000], [*Carmichael et al.*, 2002]. The uncertainties can include the interaction between the source emissions and the atmosphere, heterogeneous processing of chemical constituents, and the mixing of air masses from widely different sources.

The high time and spatial resolution for SO_2 on the P-3B clearly showed that the vertical distribution of SO_2 was often confined to layers of 200 to 300 meters deep. In addition, there were often shallow mixed layers with two layers below the boundary layer top marked by the temperature inversion. We have investigated these layers using the turbulence data, thermodynamic data, and other chemical tracers to understand the SO_2 distribution in these layers. One driving force for this study was to characterize these layers because they may be responsible for the transport of SO_2 to the central Pacific troposphere at altitudes below 4 km but above the mixed layer. *Cho et al*. [this issue] have characterized the turbulence and stability of the free troposphere from the TRACE-P TAMMS data. Their analyses supported the idea that differential

advection can maintain tracer gradients in the free troposphere. The transport occurred in layers that are bounded by thin turbulent layers, which maintain their integrity over significant distances.

Yellow Sea P-3B Missions

During TRACE-P the flight plans for the P-3B for 17-18 Mar 2001 were to execute a stair step pattern along 124.5^{o}E extending from 25^{o}N north of Taiwan into Yellow Sea as far as 37^{o}N. The chemical transport models predicted outflow from China north of 25^{o}N at altitudes from 1.3 to 4 km. The SO_2 distributions observed during these two flights along their common flight track from 29^{o}N to 38^{o}N have been analyzed in the context of the meteorological conditions to illustrate how the dynamics were affecting the SO_2 distributions. The observations were also compared to the CFORS/STEM-2K1 chemical transport model results for the same period.

On 17 Mar 2001 flight 13 of the P-3B originated in Hong Kong and executed its flight plan along 124.5^{o}E to the Yellow Sea and terminated at Kadena, Okinawa (127.75^{o}E 26.38^{o}N). On 18 Mar 2001 flight 14 of the P-3B was flown along 124.5^{o}E from the East China Sea north of Taiwan to the Yellow Sea near the Korean peninsula. The SO_2 distribution along the 124.5^{o}E meridian is shown in figure 1. A small portion of the vertical profile at 30^{o}N for flight 14 is shown in figure 1 to illustrate the downwind extent of the SO_2 advection east of 124.5^{o}E. At the end of the 150 m leg along 124.5^{o}E, the aircraft then turned east along 29.6^{o}N until it could proceed along the east coast of Japan where the flight terminated at Yokota Air Base (139.35^{o}E 35.7^{o}N).

In the region where these two flights took place weather conditions were quite different. A front passed through the area on 16-17 Mar 2001 with clear air filling in over the Yellow Sea on 18 Mar 2001. The precipitation analysis daily images for 15-18 Mar 2001 from the Tropical

Rainfall Measurement Mission (TRMM) microwave imager (TMI) [Global Precipitation Climatology Project, Laboratory for Atmospheres, NASA Goddard Space Flight Center, http://precip.gsfc.nasa.gov/rain_pages/daily_choice.html] indicated a wide area of 0.5-1 cm/day of rain from 26°N to 32°N on 16 Mar 2001. The Special Sensor Microwave Imager (SSM/I) on the Defense Meteorological Satellite program (DMSP) for 16 Mar 01 showed the same wide area of rain but the heaviest rain (8 cm/day) was centered on 125°E 30°N. The three hour images from the GMS-5 infrared channels tuned to the microwave imaging rainfall data by the Naval Research Laboratory [http://asd-www.larc.nasa.gov/David/gtewestpacprecip.html; http://www.nrlmry.navy.mil/archdat/rain_tutorial/westpac/training/index.html] showed that there was a band of 1-2 cm of rain along 34°N and with the maximum near on 125°E at 0300 UTC on 16 Mar 2001. There was no rainfall in the study area indicated by any satellite data for the two flight days.

On 17 Mar 2001 the aircraft intercepted several low-level stratus layers off the coast of China along the 124.5°E meridian. Above the P-3B flight path on 17 Mar 2001 there also were some high altitude clouds between 33°N to 38°N. On 18 Mar 2001, the study area was clear of clouds since the front had passed through the previous evening. Satellite and weather summaries are available on the GTE archive website [http://asd-www.larc.nasa.gov/David/gtetracepp3bwxpg.html].

Although the winds on both flights were from the west to northwest, the SO_2 concentrations were markedly different in vertical and horizontal distributions along 124.5°E (figure 1). The SO_2 concentrations along 124.5°E for both flights increased from south to north as predicted by the transport models. The highest SO_2 concentrations on each flight were below 2 km with the

peak SO_2 levels at or below 1 km. However, this view of the distribution (figure 1) does not indicate the high spatial and temporal variation of the SO_2 concentrations in these flight profiles.

The SO_2 concentrations for the level flight legs between the surface and 3.8 km for the flight track along 124.5^{o}E are shown in figure 2. The northern end of the track was within 160 km of the middle of the Korean peninsula, and near the southern end of flight track at 30^{o}N Shanghai was 300 km to the west. Flight 13 had concentrations about an order of magnitude lower than flight 14 below 2 km. Above 3 km both flights had SO_2 concentrations <150 pptv that appeared to have been transported from much further west than coastal China. These upper air masses were likely isolated from the air mass below as shown in the thermodynamic structure and the vertical velocity profiles in the following sections.

Flight 13

Along the 124.5^{o}E track on flight 13, the winds for the 150 m level legs were 300^o to 320^o while the winds for the 1.4 km and 2.6 km levels were 260^o to 270^o. At 150 m there appeared to be two plumes: one north of 34^{o}N and another between 32^{o}N and 33.8^{o}N (figure 2b). Between these plumes near 34^{o}N the SO_2 concentrations were 30-40 pptv, which was typical of remote North Pacific air [*Thornton et al.*, 1999]. This decrease in SO_2 at 150 m between 33.8^{o}N and 34^{o}N was likely the result of rainout and washout in the rain band described above in the tuned GMS-5 satellite image. The SO_2 concentrations of 40-70 pptv at 1.4 km between 32^{o}N and 33.3^{o}N and may have been reduced by cloud processing or rain. At 2.6 km the SO_2 levels were 200-300 pptv (figure 2a), which was comparable to the mixed layer concentrations at 33.7 ^{o}N and 34.4^{o}N. The SO_2 at 2.6 km may have been above the clouds and apparently was not as affected by rainout or washout that removed SO_2 around 34^{o}N in the mixed layer below.

At 150 m between 31°N and 33°N for flight 13, fresh ship plumes were a major local source of the SO_2 (figure 2b). The three largest SO_2 ship plumes were very fresh as there were decreases in ozone (O_3) [Avery, TRACE P data archive] as well as ppbv levels of nitric oxide (NO) [Kondo, TRACE P data archive]. An estimate of the impact of the ship plumes was made by integrating only the short period spikes in SO_2 from the ship plumes compared to the integral SO_2 concentration along this leg assuming a constant mixed layer height. By this estimate the ship plumes would account for 46% of the SO_2 along this leg. However, the mixed layer height changed from 650 m at 31.2 °N (figure 3c) to 1.2 km at 32.7 °N (figure 4c) with a cloud base of 500 m. Without knowing how extensive this cloud was along the track, it is difficult to estimate the true impact of the ship plumes for this leg. Based on these data it appears that ship plumes can have a significant impact on the mixed layer when SO_2 transported from the continent is greatly reduced by precipitation [*Streets et al.*, 2000].

In contrast to the southern mixed layer leg, the northern leg over the Yellow Sea (33.6°N to 34.8°N) did not appear to have any fresh ship plumes based on the NO and O_3 data. The decreases in SO_2 at the northern end were associated with high relative humidity implying that the SO_2 may have been removed by washout or by a cloud processing. For example, near 34.7°N SO_2 dropped from 700 pptv to 100 pptv, which was coincident with high relative humidity. The detection of droplets on the Gerber particle volume measurement (PVM) probe [Clarke, TRACE-P data archive] indicated that there might have been drizzle in this region.

The vertical profiles that bracket the mixed layer legs of flight 13 (figure 2b) illustrate the highly structured layers in the SO_2 vertical distribution (panel a of figures 3-6). The most striking feature of these vertical profiles is the layering of SO_2. The key to understanding this layered structure lies in the turbulence structure, which can be observed from the variance of the vertical

wind component from the TAMMS data [*Thornhill et al.*, this issue]. The vertical profiles of *w'* ($w' = w_i - w_{mean}$) (panel c for figures 3-6) more clearly delineate the mixed layers than the vertical profiles of water vapor mixing ratio (panel d for figures 3-6) or equivalent potential temperature (θ_e) (panel e for figures 3-6) The well-mixed part of the boundary layer is indicated by the large variance in *w'*, which reflects the large range in eddy scales that existed. When the variance is very small there is, in effect, a very low rate of vertical or horizontal mixing. The variance in *w'* is also useful in determining if the boundary layer consisted of a well mixed lower layer and an intermittently mixed upper layer [*Russell et al*., 1998, *Wang et al*., 1999]. The liquid water content (LWC) derived from the PVM probe clearly marked the presence of the cloud layers for flight 13 (panel f for figures 3-6).

North of 30^{o}N the wind had a more northerly component to the general westerly flow of the southern end of the track. The back trajectories indicated air had passed over Northern China and then along the western side of the Korean peninsula (figure 7). At 31^{o}N the SO_2 layer with 1 ppbv between 700 and 900 m (figure 3a) was below the layer of high CO from 1.1 to 2.1 km (figure 3b). This SO_2 plume was constrained between a weak inversion at 900 m (figure 3e) and the well mixed layer below 600 m (figure 3c). At the top of the mixed layer there was a thin cloud layer, which was indicated by the liquid water content (figure 3f). The back trajectories near 1 km for this SO_2 layer (triangles in figure 7) descended from above 3 km from the northwest and were over the sea off Shanghai for the day before the flight.

Between 1.2 km and 2 km, where CO exceeded 500 ppbv, the back trajectories descended near the surface over southern China 2-3 days earlier, but the SO_2 concentrations of 20-40 pptv were more like those in the mixed layer. With a cloud at 1.8 to 2 km (figure 3f) and the MR between 1.3 and 2.1 km greater than in the mixed layer, it appeared that there had been rain

earlier that reduced the SO_2 levels compared to the fresh SO_2 plume from Shanghai between 700 and 900 m. Above the cloud SO_2 was 60-80 pptv in a region of low turbulence (figure 3c) and much more stable air (figure 3e) where CO values were near 200 ppbv. The air above 2 km also had back trajectories to southern China.

The effects of clouds on the SO_2 distribution are illustrated by the vertical profiles at 32.7^o N, 33.6^{o}N, and 34.8^{o}N (figure 4a, 5a, 6a). The wettest cloud encountered on flight 13 was at 32.7^{o}N (figure 4f). The turbulence data showed that the mixing extended to the cloud top and that the cloud was convective because there were a number of large positive excursions of *w'* (figure 4c). The spikes in SO_2 in this profile between 400 m and 1 km are positively correlated to the positive excursions of *w'*. The largest of these updrafts at 1 km corresponded to an SO_2 concentration the same as in the lower part of the mixed layer below 400 m. An air parcel with an updraft velocity of 2 m/s would have a transit time of about 5 min from the lower mixed layer at 400 m to 1 km.

At 33.6^{o}N (figure 5a) a similar situation was encountered where the cloud had nearly dissipated (LWC $\leq$0.1 g/m^3, figure 5f). Below 400 m SO_2 is greater than 200 pptv in the mixed layer (figure 5a), but there were a number of updrafts, which could have produced the structure in the SO_2 profile. Above 400 m the turbulence was less intense (figure 5c), but the structure in the SO_2 profile up to 700 m was probably the residual from the convection in the cloud that was dissipating. Drier, less turbulent air with lower CO was above the cloud top at 700 m and appeared to be diluting the moister CO-richer air below causing the cloud to dissipate. At 200 m the SO_2 increased from 200 pptv to 280 pptv, which was what was found on the level leg after the descent. Small jumps in the MR and CO also occurred at 200 m and the concentrations be-

came more uniform below 200 m, which would be expected in the mixed layer. It appeared that the mixed layer had reestablished at a lower altitude after the cloud began to dissipate.

At the northern end of the 150 m leg over the Yellow Sea there were clouds extending from 200 m to 1.7 km. Two breaks in the cloud are apparent at 350 m and 1.5 km where the LWC was near zero (figure 6f). The SO_2 below 400 m varied between 800 to 1000 pptv, and above 400 m SO_2 linearly declined to a minimum of 30 pptv at 1 km. At 1.1 km CO also decreased from 210 ppbv to 130 ppbv (figure 6b) and NO went from >200 pptv to <20 pptv. Although there was a wind shear of 60 degrees from northwest to west at 1.1 km, the air composition appeared more like Northern Hemisphere oceanic air. The back trajectory for 1.3 km indicated that the air had been in the region of the Korean Strait to the east for 2 days (diamond symbol in figure 7). It is likely that this air mass had been lifted up over the front from the west as part of the warm conveyor belt mechanism [*Jacob et al*., this issue]. A similar condition had been observed east of Taiwan during PEM West A where the mixed layer was polluted but the air just above was typical of clean marine air from the southeast [*Thornton et al*, 1996].

Flight 14

On 18 Mar 01 the front had cleared the region of the Yellow Sea and the East China Sea, and there were no clouds along the 124.5^{o}E flight path. The peak SO_2 levels were an order of magnitude greater compared to the previous day. At 36^{o}N 2-10 ppbv of SO_2 was distributed in several layers from near the surface to 2.5 km. At 30^{o}N SO_2 had decreased to <2 ppbv below 600 m. A distinct plume of SO_2 was observed between 200 m and 300 m from 31^{o}N and 36^{o}N. A similar plume of CO at those altitudes was observed between 34^{o}N and 36^{o}N, which may indicate a common source.

The structure of the lower atmosphere for the track along the 124.5^{o}E meridian was very complex. Colder air was descending over 36^{o}N, but at 150 m the air was warmer than the sea surface temperature creating a stratified boundary layer (figure 8e). Between 35^{o}N and 36^{o}N the aircraft was not completely in the mixed layer at 150 m. At the southern end of the track near 30^{o}N, the sea surface temperature was higher than the air temperature and a well developed mixed layer was established with a depth of 600 m (figure 11c, 11d) similar to the previous day (figure 3c, 3d).

The lower troposphere was unstable at 36^{o}N (figure 8e) with 5 inversions below 2.5 km. Between the inversions at 0.8 and 1.7 km SO_2 was a nearly constant at 6 ppbv (figure 8a). This layer appeared to be constrained between the inversions at 800 m and 1.7 km and the profiles of CO (figures 8b), water vapor (figure 8e), and ozone also had abrupt changes at these two altitudes. The slow meandering of *w'* in this layer was more characteristic of the free troposphere than the boundary layer.

The distinct plume of SO_2 and CO between 600 and 800 m (figure 8a, 8b) also contained NO> 200 pptv, indicating a fresh pollution plume. This air was also nearly 50% moister than the air above or below (figure 8d). The plume appeared to be trapped between the inversion at 800 m and a shear layer near 600 m, which is reflected in *w'* (figure 8c). These northern SO_2 plumes at 36^{o}N all had back trajectories to the Hebei region in one day (figure 12 down triangle and right pointing triangle symbols).

From 31^{o}N to 36^{o}N a well defined SO_2 layer existed between 200 m and 300 m (figure 8a, 9a, 10a). This plume was below the inversions that were near 400 m at 31^{o}N and 300 m at 35.7^{o}N (figure 8e, 9e, 10e). Between 34^{o}N and 35.7^{o}N the fight path did not descend low enough to remain in the mixed layer. It is clear from the turbulence (figure 9c, 8c) and θ_e (figure 9e, 8e)

that the flight path was still above the mixed layer at 150 m. The sea surface temperature had decreased 2 K between 31^{o}N and 36^{o}N while the air temperature remained nearly the same. North of 35^{o}N the air temperature was greater than the sea surface temperature. With the warmer air above the colder sea this part of the boundary layer became stable, particularly between 34^{o}N and 36^{o}N, where the turbulence below 400 m (figure 8c, 9c) is more like the free troposphere than a well mixed boundary layer. Based on the turbulence data (figures 8c, 9c) and the MR data (figure 8d, 9d), it appeared that the aircraft did not descend low enough to be completely in the mixed layer at 150 m between 35^{o}N and 36^{o}N. The high variability observed for SO_2 on the level leg at 150 m at 35.4^{o}N (figure 2d) was probably caused by the aircraft path going in and out of the mixed layer and the plume above the mixed layer top.

At 34.2^{o}N θ_e indicated an air mass above 1 km with neutral stability (figure 9e). Both SO_2 and CO between 1 and 1.7 km at 34.2^{o}N (figure 9a, 9b) were half their concentrations at 36^{o}N. The back trajectories for the SO_2 between 1 and 2 km all passed north of the Shandong peninsula (37^{o}N), but the air parcels descended from above 3 km to the aircraft position. The air parcels below 1 km on the aircraft track had come from the region of 115^{o}E 35^{o}N within 1.5 days and remained below 1.5 km (figure 12 square symbol). That region contains three major point sources in southern Shandong and northwestern Jiangsu [*Streets et al*., this issue].

At 31.1^{o}N the turbulent mixing was stronger below 400 m, but in this area the flight path appeared to be crossing through a sloped mixed layer top that was uneven. Based on the rapid oscillations in SO_2, *w'*, θ_e (figure 10 below 200 m) and the Lyman α fast water vapor sensor, the flight path was probably in and out of the top of the mixed layer. There was a sharp drop in SO_2 from 8 ppbv above 200 m to about 4 ppbv below 200 m (figure 10a). It appeared that SO_2 from the plume between 200 and 400 m was isolated from the mixed layer.

Between 31.1°N and 30.2°N SO_2 at 150 m steadily decreased from 3 ppbv to 1.5 ppbv (figure 2d). At the southern end of the flight track at 30°N the mixed layer was 600 m deep (figure 11b, 11d, 11e) compared to about 200 m at 31°N. The decrease in SO_2 from 31°N to 30°N at 150 m was related in part to the increase in the mixed layer depth (figure 10b, 11b). The sea surface temperature had increased by 2 K from the north to the south, which would have increased the heating of the mixed layer.

The vertical profile at 30°N was to the east of the 124.5°E meridian at the end of the flight pattern in this region. There was a well defined top to the mixed layer (figure 11c, 11d) where there was a sharp decrease in SO_2 (figure 11a) and the very stable air mass above 600 m (figure 11e) where SO_2 decreased to 40 pptv. The SO_2 plume between 1.4 km and 1.6 km at 30° N (figure 11a) was in an air mass of neutral stability (figure 11e) with very low turbulence (figure 11c). The structural features of this SO_2 profile were also present for O_3 (figure 11b) and NO, and water vapor had decreased to <0.6 g/kg compared to >1 g/kg above 1.6 km and >2.5 g/kg below 1.3 km. Based on the back trajectories, the SO_2 plume at 30°N came from the southern side of the Shandong peninsula (figure 12 circle symbol). The back trajectories indicated air parcels that rapidly descended from above 3 km, which is consistent with θ_e >320 K above 1.5 km at 30°N (figure 11e). This descending air mass appeared to have trapped and constrained the SO_2 pollution plume.

4. Discussion

The transport of SO_2 for these 2 flights over the East China Sea -Yellow Sea region was very varied within the boundary layer as well as above it. Transport occurring above the boundary layer is not surprising given the convective activity of early spring over the East Asia basin

and the generally westerly winds [*Fuelberg at al*., this issue]. However, the transport was often in well defined layers that were constrained by the lack of vertical mixing and by the thermodynamic structure. These plumes appeared to maintain their structure well away from the coast of Asia under conditions described by *Cho et al*. [this issue] and *Thornton et al*. [2002b].

The most unusual part of the SO_2 plume structure was just above the mixed layer top and in the mixed layer. For these two flights with greatly different SO_2 concentrations, the structure of boundary layer was also different. There was a well mixed layer close to the sea surface for both flights but the depth was much less for flight 14 except at 30^oN. The greater depth (600 – 1000 m) for flight 13 was related to the clouds of varying heights. Above the well mixed layer there was a less well mixed layer but still below a temperature inversion or a major decrease in water vapor that usually marks transition to the free troposphere.

During flight 13 the SO_2 was found to be transported from the continent in the well mixed layer as well as in cloud but in decreasing amounts from the Yellow Sea in the north to the East China Sea in the south. The SO_2 observed in clouds was mixed by convection into the cloud from the SO_2 rich air below. One of the limits to SO_2 uptake in cloud is the availability of hydrogen peroxide (H_2O_2). With ppbv levels of SO_2 at the northern end, heterogeneous loss of SO_2 to cloud droplets may have been limited by the depletion of H_2O_2 by the SO_2. The remaining primary loss process is by O_3, which has limited solubility in water and a much lower rate of reaction. It is difficult to assess the cloud loss rate of SO_2 because this experiment was not designed to study clouds so that the effects of dilution could not be ascertained.

The SO_2 plumes in the lower free troposphere of flight 13 were like the plumes above the well mixed layer for flight 14. In both cases the plumes were in air masses with lower turbulence and with high to neutral stability. The SO_2 plumes at 31^oN and 32.7^oN (figures 3a, 4a) may have

been the leading edge of the air mass filling in behind the front that cleared the region late in the day. This air mass movement was above the stratus cloud decks although it may have been affected by precipitation on the previous day.

During flight 14 over the Yellow Sea it appeared that the transport from surface sources near the coast occurred when the continental air moved offshore over the marine boundary layer. The marine mixed layer depth (<150 m) was constrained by the cold surface temperature and the warmer air above (figure 8e, 9e). Even though it was early spring, the continental boundary layer was deeper than the marine boundary layer because the highly populated land mass contributed to the diabatic heating over land. The structure of the plumes north of 31^{o}N was related to the turbulence structure between 200 m and 1000 m (figure 8c, 9c, 10c). The apparent oscillations in the SO_2 (figure 8a, 9a, 10a) were also seen for O_3 and NO. These oscillations corresponded to the meanders of the vertical velocity (figure 8c, 9c, 10c). The other extreme in turbulence is seen in the region between 450 and 750 m (figure 9c) where the turbulence mixed the chemical species to nearly uniform concentrations in this layer (figure 9a, 9b).

The observation that transport between the mixed layer and the layer above can be dynamically limited introduces a possible scenario of why SO_2 can persist in low level plumes over the ocean *Thornton et al*. [2002b]. When the vertical transport is controlled by entrainment processes, then mixing occurs on much slower time scales than when mixing is determined by convection. When entrainment is controlling the transport of SO_2 to the sea surface, the loss of SO_2 to sea salt aerosol near the surface and to the surface itself becomes limited. If this dynamic control is not included in transport models, an overestimation of SO_2 heterogeneous loss to the sea or aerosol would be likely. The same would be true when the SO_2 plumes are just above the boundary layer top where the mixing processes appeared to be limited by the colder air masses

descending over the marine boundary layer. Investigation of these possibilities for contributing to long range transport over the Pacific will be presented separately.

By looking at the ethyne (C_2H_2) [Blake, TRACE P data archive] to CO ratio we can get an estimate of the age of the air relative to its photochemical decay and dilution by mixing [*McKeen and Liu*, 1993; *McKeen et al.*, 1996; *Sandholm et al.*, 1992, 1994; *Smyth et al*., 1996]. Above 2.5 km the relationship of SO_2 to the C_2H_2/CO was similar for both flights. For the most recent encounters of the pollution plumes (C_2H_2/CO>3), SO_2 was increasing with increasing C_2H_2/CO (figure 13a, c). These SO_2 samples were all from the region north of 33^{o}N. When C_2H_2/CO was <3 above 2.5 km, SO_2 was generally <50 pptv. For flight 13 the low SO_2 concentrations with C_2H_2/CO >3 were consistent with SO_2 being significantly reduced by heterogeneous processing by precipitation and clouds on the day prior to the encounter with the aircraft. The low SO_2 values for flight 14 with C_2H_2/CO <3 were all from the region south of 32^{o}N. While the lower values of C_2H_2/CO indicate longer time for processing, the low SO_2 concentrations may have been reduced by the cloud and heterogeneous processing during the periods of precipitation between 27^{o}N and 32^{o}N over the sea on 15 Mar 01, two days before the encounter with the aircraft.

Below 2.5 km heterogeneous processing of SO_2 by clouds, precipitation, and sea salt aerosol, and the sea surface would be more likely. This is clearly seen for flight 13 at all values of C_2H_2/CO when SO_2 was <100 pptv (figure 13b). For the northern end of the flight track in the Yellow Sea, the SO_2 concentrations >200 pptv were in the plume moving from north to south (figure 2b) with C_2H_2/CO between 3.5 and 4, which would have been within one day of transport from the source to the encounter with the aircraft. A similar relationship of SO_2 with C_2H_2/CO was seen for flight 14 when all of the plumes below 2.5 km described above were within 1.5

days transport from the source (figure 12). Here the range of SO_2 concentrations more likely represents the source variations.

5. Model comparison

The CFORS/STEM-2K1 modeling system as used in the Trace-P and Ace-Asia experiments was built within the RAMS mesoscale meteorological model [*Pielke et al.*, 1992]. The CFORS component contained multiple tracers run on-line in RAMS, so that all the on-line meteorological information such as three dimensional (3-D) winds, boundary-layer turbulence, surface fluxes and precipitation amount are directly used by the tracer model at every time step. As a result, CFORS produces with high time resolution 3-D fields of tracer distributions and major meteorological parameters. For the analysis of reactive species, a chemical transport model (CTM) is used. In this paper we discuss results using the STEM model. The STEM version used is referred to as the 2K1 (2001) version (thus STEM-2K1). CFORS provides the meteorological fields used by STEM, and then STEM calculates the transport, chemistry, removal, and photolysis processes. The important new features in STEM-2K1 include: i) the use of the SAPRC99 chemical mechanism [*Carter*, 1999], which consists of 93 species and 225 reactions; ii) the integration of the chemical mechanism using and the implicit second order Rosenbrock method [*Verwer et al*., 1997]; iii) the calculation of photolysis rates on-line, considering the influences of cloud, aerosol and gas-phase absorptions due to O_3, SO_2 and NO_2, using the NCAR Tropospheric Ultraviolet-Visible (TUV) radiation model [*Madronich*, 1999]; and iv) the extension of the aerosol calculations to include optical information (e.g., extinction) in addition to mass, size and composition. Complete details regarding this model are available in *Carmichael et al*., [this is-

sue], and *Uno et al*., [in press]. Boundary conditions were selected based on observational data, and they were set to the lowest 5% at each altitude of the values observed during the Trace-P operations in the western Pacific. The numerical model domain for the analysis (both CFORS and STEM) was centered at 25^{o}N 115^{o}E with a horizontal grid of 100 by 90 grid points and a resolution of 80 km. In the vertical, the domain was divided into 23 layers (non-uniformly spaced layers ranging in depth from 150 m to 1800 m), with the top level at 23km. All calculations were performed on Linux clusters.

The SO_2 observations and the results of the CFORS/STEM-2K1 model [*Carmichael et al.,* this issue] along the path for the entire P-3B flight 13 are shown in figure 14. The time period when the flight track was along 124.5^{o}E is 0315 to 0805 UTC. The model closely followed the SO_2 data at all altitudes before 0400 UTC, which was mostly in the area between Hong Kong and Taiwan. That region had not received any precipitation for at least 4 days prior to the flight [Global Precipitation Climatology Project, Laboratory for Atmospheres, NASA Goddard Space Flight Center, http://precip.gsfc.nasa.gov/rain_pages/daily_choice.html]. .

After 0400 UTC, the model results exceeded the SO_2 observations at all altitudes by factors of 2 to 20. The vertical distribution of the model had SO_2 >0.5 ppbv at all altitudes above 0.5 km between 0430 and 0530 UTC which were not observed. Between 0600 and 0730 UTC the model trend was the same as the observations, but the model results were higher by an order of magnitude compared to the observations. As described above, the observations indicate that a large fraction of SO_2 had likely been removed by heterogeneous processing prior to flight 13, particularly below 2 km.

Near the end of flight 13, away from the flight track in the Yellow Sea, the model had SO_2 concentrations near 1 ppbv at 3.1 km while the observations were that the SO_2 was 0.1 ppbv.

Above 3 km the model results were <100 pptv, but the observations showed a 500 pptv layer about 4.4 km with concentrations above and below of >200 pptv. The model accurately predicted the 250 ppbv CO for the 3 km leg, but it under predicted the 100 ppbv CO and the 55 ppbv ozone at 5.5 km. The SO_2 concentrations of 200 pptv at 5.5 km were much higher than expected based on the C_2H_2/CO ratio of 1.3 for other data along 124.5°E (figure 2a). Most of the back trajectories at 5.5 km passed over northern India above 5 km two days earlier and descended to 2-4 km over central and southern Sudan five days earlier. The only likely significant SO_2 source would be oil refineries in central Sudan and in the oilfields of southern Sudan. This would be consistent with the C_2H_2/CO ratio and the 0.5% sulfur content of the oil [http://www.eia.doe.gov/emeu/cabs/sudan.html]. In this case the source was out of the model domain for this field study.

The model gave better agreement with the SO_2 observations on flight 14, particularly on the flight legs below 1 km. The model significantly overestimated the SO_2 for the 1.5 to 2.5 km levels. One low level feature the model missed was the decrease in SO_2 as the flight path turned east from 124.5°E toward Japan (about 0600 UTC in figure 15). The model similarly overestimates SO_2 on a 150 m leg off the coast of Japan at 0800 UTC, although the model accurately predicted the 240 ppbv of CO.

If precipitation was the primary cause of the model overestimating the SO_2 for flight 13, the model should have done better on flight 14 for those altitudes between 1.5 and 2.5 km. We believe that the dynamics (described above) resulted in this deviation. At the northern end of the Yellow Sea flight path (0330-0400 UTC), the model exceeded the SO_2 observations by a factor of 3-4 (figure 15). Near 2 km on either side of the southern 150 m leg (0500-0530 UTC and 0615-0645 UTC) the model overestimated the observed SO_2 by a factor of 7-10. It appears that

the model did not capture the dynamics properly and expanded to higher altitude the plumes that lay below 2 km. At the northern end the profile showed unstable regions capped by inversions with enhanced turbulence just below 2 km (figure 8c). At the southern end the atmosphere had neutral stability but there was virtually no turbulence. With no turbulence it would be less likely that the 200 m thick SO_2 plume at 1.5 km (figure 11a) would be diffused [*Cho et al.*, this issue]. Here the scale of the SO_2 feature was too small for the model resolution.

The reasons for the poorer performance of the model under cloudy conditions remain an open question. However, from detailed analysis of model performance related to photochemical processes, including the calculation of photolysis rates and a number of the species active within the photochemical oxidant cycle (e.g., OH, HCHO, PAN, O_3), this problem does not appear to be associated with deficiencies in the gas phase mechanism. It is possible that there are some issues related to cloud chemistry, however, the fine-scale turbulence structure that was observed was not adequately resolved in our present modeling analysis. A more detailed treatment of the dynamics in the continental/marine transition region, and finer vertical resolution in the CFORS meteorological analysis, are required to more accurately capture this behavior. This line of study is now underway.

6. Conclusion

During the P-3B flights over the Yellow Sea much of the transport and distribution of SO_2 can be understood in the context of the dynamics and thermodynamics of the atmosphere. As might be expected, the meteorological complexity is high during the transition from winter to early spring near the coast of the East Asian continent because of the differences in temperature

between land and sea and frequent frontal passage. It was clear that precipitation near the coast had a major effect on decreasing SO_2 transported to the Pacific Ocean at low altitudes. However, in the air masses following frontal passage, significant amounts of SO_2 were transported between 0.5 and 2 km.

In the subsiding air behind the front, high concentrations of SO_2 were transported significant distances above the marine mixed layer. The SO_2 transport occurred in layers defined by low turbulent mixing that were often constrained by temperature inversions. In several cases discussed here, SO_2 layers were immediately above the marine mixed layer. In the absence of convective mixing, the relatively slow process of entrainment limited the transport of SO_2 into the marine mixed layer and, consequently, to heterogeneous loss to the sea surface and sea salt aerosols. Further investigation of the TRACE-P data is underway to evaluate the role of the atmospheric dynamics in the long range transport of Asian SO_2 across the North Pacific.

When the CFORS/STEM-2K1 regional scale chemical transport model is compared to observations over a two day period that represented the extremes of the spring transport, it was clear that the poor agreement was related to the treatment of the dynamics on the SO_2 distributions. Some features were on scales that were not within the resolution of the model. The major deviations of the model from the observations were in the mixed layer on the day of the frontal passage and in the 1.5 to 2.5 km range for both wet and dry conditions.

Acknowledgement. We gratefully acknowledge support of the NASA GTE program under grant NCC-1-409, TAMMS group at NASA Langley Research Center for their excellent cooperation in data acquisition and processing, the GTE Project office for their assistance throughout the mission, and the NASA Wallops Flight Facility crew of the P-3B for their assistance during the field mission.

References

Bandy, A.R., D.C. Thornton, and A.R. Driedger, III, Airborne measurements of sulfur dioxide, dimethyl sulfide, carbon disulfide, and carbonyl sulfide by isotope dilution gas chromatography/mass spectrometry, *J. Geophys. Res.*, *98* (D12), 23423-33, 1993.

Carmichael, G.R., G. Calori, H. Hayami, I. Uno, S.Y. Cho, M. Engardt, S.B. Kim, Y. Ichikawa, Y. Ikeda, J.H. Woo, H. Ueda, and M. Amann, The MICS-Asia study: model intercomparison of long-range transport and sulfur deposition in East Asia, *Atmos Environ, 36* (2), 175-199, 2002.

Carmichael, G.R., Y. Tang, G. Kurata, I. Uno, D.G. Streets, J.-H. Woo, H. Huang, J. Yienger, B. Lefer, R.E. Shetter, D.R. Blake, A. Fried, E. Apel, F. Eisele, C. Cantrell, M.A. Avery, J.D. Barrick, G.W. Sachse, W.L. Brune, S.T. Sandholm, Y. Kondo, H.B. Singh, R.W. Talbot, A.R. Bandy, A.D. Clarke, and B.G. Heikes, Regional-scale chemical transport modeling in support of intensive field experiments: overview and analysis of the TRACE-P observations, this issue.

Carter, W., Documentation of the SAPRC-99 chemical mechanism for voc reactivity assessment, Final Report to California Air Resources Board Contract No. 92-329, University of California-Riverside, May 8, 2000. Madronich, S. and Flocke, S., The role of solar radiation in atmospheric chemistry, in *Handbook of Environmental Chemistry* (P. Boule, ed.), Springer-Verlag, Heidelberg, 1-26, 1999.

Chin, M., D.L. Savoie, B.J. Huebert, A.R. Bandy, D.C. Thornton, T.S. Bates, P.K. Quinn, E.S. Saltzman, and W.J. DeBruyn, Atmospheric sulfur cycle simulated in the global model GOCART: Comparison with field observations and regional budgets, *J. Geophys. Res. Atmos.*, *105* (D20), 24689-24712, 2000.

Cho, J.Y.N., R.E. Newell, B.E. Anderson, J.D.W. Barrick, and L.K. Thornhill, Characterizations of tropospheric turbulence and stability layer from aircraft observations, *J. Geophys. Res.*, this issue.

Fuelberg, H. E., R. O. Jr. Loring, M. V. Watson, M. C. Sinha, K. E. Pickering, A. M. Thompson, G. W. Sachse, D. R. Blake, M. R. Schoeberl, TRACE A trajectory intercomparison, 2, Isentropic and kinematic methods, *J. Geophys. Res*., 101, (D19), 23927-23939, 1996.

Fuelberg, H.E., C.M. Kiley, J. R. Hannan, D. J. Westberg, M. A. Avery, R. E. Newell, Atmospheric transport during the transport and chemical evolution over the Pacific (TRACE-P) experiment, *J. Geophys. Res.*, this issue.

Hoell, J.M., D.D. Davis, S.C. Liu, R. Newell, M. Shipham, H. Akimoto, R.J. McNeal, R.J. Bendura, and J.W. Drewry, Pacific exploratory mission-west A (PEM-West A): September-October 1991, *J. Geophys. Res.*, *101* (D1), 1641-53, 1996.

Hoell, J.M., D.D. Davis, S.C. Liu, R.E. Newell, H. Akimoto, R.J. McNeal, and R.J. Bendura, The pacific exploratory mission-west phase B: February-March, 1994, *J. Geophys. Res.*, *102* (D23), 28223-28239, 1997.

Kim, B-G, J-S. Han, and S-U Park, Transport of SO_2 and aerosol over the Yellow Sea, *Atmos. Environ.*, 35, 727-737, 2001.

Jacob, D.J., J.H. Crawford, M.M. Kleb, V.E. Connors, R.J. Bendura, and J.L. Raper, The Transport and chemical evolution over the Pacific (TRACE-P) mission: design, execution, and overview of results, *J. Geophys. Res.*, this issue.

Madronich, S. and Flocke, S., The role of solar radiation in atmospheric chemistry, in Handbook of Environmental Chemistry (P. Boule, ed.), Springer-Verlag, Heidelberg, 1-26, 1999.

McKeen, S. A. and S. C. Liu, Hydrocarbon ratios and photochemical history of air masses,*Geophys. Res. Lett., 20,* 2363-2366, 1993.

McKeen, S. A., S. C. Liu, E. –Y. Hsie, X. Lin, J. D. Bradshaw, S. Smyth, G. L . Gregory, and D. R. Blake, Hydrocarbon ratios during PEM-West A: A model perspective, *J. Geophys. Res., 101,* 2087-2109, 1996.

Pielke, R. A., Cotton, W. R., Walko, R. L., Tremback, C. J. , Lyons, W. A., Grasso, L. D., Nicholls, M. E., Moran, M. D., Wesley, D. A., Lee , T. J. and Copeland, J. H., A comprehensive meteorological modeling system-RAMS, Meteorol. Atmos. Phys., 49, 69-91, 1992.

Russell, L. M.; D. H. Lenschow, K. K. Laursen, B. Krummel, S. T. Siems, A. R. Bandy, D. C. Thornton, T. S. Bates, Bidirectional mixing in an ACE 1 marine boundary layer overlain by a second turbulent layer, *J. Geophys. Res.*, **103**, 16,411-16,432, 1998.

Sandholm, S. T., et al., Summertime tropospheric observations related to N_xO_y distributions and partitioning over Alaska: ABLE 3A, *J. Geophys. Res., 97,* 16,481-16,509, 1992.

Sandholm, S. T., et al. Summertime partitioning and budget of NO_y compounds in the troposphere over Alaska and Canada: ABLE-3B, *J. Geophys. Res., 99,* 1837-1861, 1994.

Smyth, S., et al., Comparison of western Pacific air mass classification schemes for the PEM-West A experiment, *J. Geophys. Res., 101(D1),* 1743-1762, 1996.

Streets, D.G., S.K. Guttikunda, and G.R. Carmichael, The growing contribution of sulfur emissions from ships in Asian waters, 1988-1995, *Atmos Environ, 34* (26), 4425-4439, 2000.

Streets, D.G., T.C. Bond, G.R. Carmichael, S.D. Fernandes, Q. Fu, D. He, Z. Klimont, S.M. Nelson, N.Y. Tsai, M.Q. Wang, J.-H. Woo, and K.F. Yarber, An inventory of gaseous and primary aerosol emissions in Asia in the year 2000, *J. Geophys. Res.*, this issue.

Thornhill, L.K., B.E. Anderson, J.D.W. Barrick, D.R. Bagwell, R. Friesen, and D.H. Lenschow, Air motion intercomparison flights during TRACE-P / ACE-ASIA, *J. Geophys. Res.*, this issue.

Thornton, D.C., A.R. Bandy, B.W. Blomquist, D.D. Davis, and R.W. Talbot, Sulfur dioxide as a source of condensation nuclei in the upper troposphere of the Pacific Ocean, *J. Geophys. Res., 101* (D1), 1883-90, 1996.

Thornton, D.C., A.R. Bandy, B.W. Blomquist, R.W. Talbot, and J.E. Dibb, Transport of sulfur dioxide from the Asian Pacific Rim to the North Pacific troposphere, *J. Geophys. Res., 102* (D23), 28489-28499, 1997.

Thornton, D.C., A.R. Bandy, B.W. Blomquist, A.R. Driedger, and T.P. Wade, Sulfur dioxide distribution over the Pacific Ocean 1991-1996, *J. Geophys. Res., 104* (D5), 5845-5854, 1999.

Thornton, D.C., A.R. Bandy, F.H. Tu, B.W. Blomquist, G.M. Mitchell, W. Nadler, and D.H. Lenschow, Fast airborne sulfur dioxide measurements by atmospheric pressure ionization mass spectrometry (APIMS), *J. Geophys. Res.*, *107*,D22, 4632, doi:10.1029/2002JD002289, 2002a.

Thornton, D.C., F.H. Tu, A.R. Bandy, M. Kim, L. Thornhill, J. D. Barrick, B. Anderson, Dynamics of Sulfur Dioxide in the Marine Boundary During TRACE-P, *AGU Transactions EOS*, 2002 Fall Meeting, 6-10 December 2002b.

Uno, I., Carmichael, G.R., Streets, D.G., Tang, Y., Yienger, J.J., Satake, S., Wang, Z., Woo, J.-H., Guttikunda, S., Uematsu, M., Matsumoto, K., Tanimoto, H.,Yoshioka, K., and Iida,T., Regional Chemical Weather Forecasting using CFORS; Analysis of Surface Observation

at Japanese Is-land Station during the ACE-Asia Experiment, J. Geophys. Res, J. Geophysical Research, 2002, in press

Venzke E, R. W. Wunderman, L. McClelland, T. Simkin, J. F. Luhr, L. Siebert, and G. Mayberry, eds., Global Volcanism, 1968 to the Present. Smithsonian Institution, Global Volcanism Program Digital Information Series, GVP-4 http://www.volcano.si.edu/gvp/reports/, 2002-

Verwer, J. G., Spee, E.J. , Blom, J.G. and Hundsdorfer, W.H.,A second order Rosenbrock method applied to photochemical dispersion problems. Modeling, Analysis and Simulation (MAS), MAS-R9717, August 31, 1997.

Wang, Q., Lenschow, D. H., Pan, L., Schillawski, R. D., Kok, G. L., Prévot, A. S. H., Laursen, K., Russell, L. M., Bandy, A. R., Thornton, D. C., Suhre, K., Characteristics of the marine boundary layers during two Lagrangian measurement periods, 2, Turbulence structure, *J. Geophys. Res*., **104**, p. 21,767-21,77, 1999.

Figure Captions

Figure 1. Sulfur dioxide distributions along the 124.5^{o}E flight path for TRACE-P P-3B flight 13 during frontal passage and flight 14 behind the front. The profile just south of 30^{o}N for flight 14 as the aircraft turned east from the 124.5^{o}E track illustrates the downwind advection of SO_2.

Figure 2. Sulfur dioxide distribution along 124.5^{o}E for the level legs for flights 13 and 14. a) and c) above the mixed layer, b) in mixed layer with spikes of SO_2 to 3 ppbv from ship plumes from 31.2^{o}N to 32.5^{o}N, d) in the mixed layer for 30-31^{o}N and in and out of the mixed layer between 34-36^{o}N.

Figure 3. Vertical ascent profiles of SO_2, CO, *w'* (the vertical wind component about the mean vertical wind for the profile shown), water vapor mixing ratio (MR), equivalent potential temperature (θ_e), and liquid water content (LWC) near 124.5^{o}E 31.2^{o}N for flight 13. Data are 1 Hz except for 10 Hz *w'* and 0.2 Hz LWC. SO_2 plume above the mixed layer top at 650 m, which is indicated by where the large variance in *w'* decreases. Cloud is indicated by the LWC at 600 m and 2 km.

Figure 4. Vertical descent profiles of SO_2, CO, *w'* (the vertical wind component about the mean vertical wind for the profile shown), water vapor mixing ratio (MR), equivalent potential temperature (θ_e), and liquid water content (LWC) near 124.5^{o}E 32.7^{o}N for flight 13. Data are 1 Hz except for 10 Hz *w'* and 0.2 Hz LWC. Note the largest SO_2 concentrations between 0.5 and 1 km that corresponded to positive excursions in *w'*, and at 1 km the SO_2 concentration was the same as below 400 m.

Figure 5. Vertical descent profiles of SO_2, CO, *w'* (the vertical wind component about the mean vertical wind for the profile shown), water vapor mixing ratio (MR), equivalent potential temperature (θ_e), and liquid water content (LWC) near 124.5°E 33.6°N for flight 13. Data are 1 Hz except for 10 Hz *w'* and 0.2 Hz LWC. SO_2 appeared to have been lost to heterogeneous processes in cloud above 500 m. Drier, less turbulent air with lower CO was above cloud top at 700 m and appeared to be diluting the moister CO-richer air below causing the cloud to dissipate (see back trajectory with circles in figure 7).

Figure 6. Vertical ascent profiles of SO_2, CO, *w*' (the vertical wind component about the mean vertical wind for the profile shown), water vapor mixing ratio (MR), equivalent potential temperature (θ_e), and liquid water content (LWC) near 124.5°E 34.8°N for flight 13. Data are 1 Hz except for 10 Hz *w'* and 0.2 Hz LWC. SO_2 appeared to be lost in cloud below 1 km but for 1 to 1.8 km lower CO compared to above and below indicated an air mass with a different origin (see back trajectory diamonds in figure 7).

Figure 7. Back trajectories for flight 13 from selected points along the 124.5°E flight relating to the vertical profiles of figures 3 to 6: triangles: 31.2°N 800 m, squares: 32.7°N 2 km, circles: 33.6°N 500 m, diamonds 34.8°N 1.2 km. Largest regions of SO_2 emissions by rank [*Streets et al.*, this issue]: 1- Shandong, 2-Sichuan, 3-Shanxi, 4-Hebei, 5-Henan, 6-Jiangsu, 7-Guizhou, 8-Liaoning, 9-Shaanxi, 10-Guangdong.

Figure 8. Vertical ascent profiles of SO_2, CO, *w'* (the vertical wind component about the mean vertical wind for the profile shown), water vapor mixing ratio (MR), and equivalent potential temperature (θ_e) near 124.5^{o}E 35.7^{o}N for flight 14. Data are 1 Hz except for 10 Hz *w'*. Note that the mixed layer appeared to be below the aircraft at the start of the ascent at 150 m. The air temperature at 150 m was greater than the sea surface temperature.

Figure 9. Vertical descent profiles of SO_2, CO, *w'* (the vertical wind component about the mean vertical wind for the profile shown), water vapor mixing ratio (MR), and equivalent potential temperature (θ_e) near 124.5^{o}E 34.2^{o}N for flight 14. Data are 1 Hz except for 10 Hz *w'*. Based on the MR and θ_e the mixed layer top was very near 150 m but the variance in *w'* does not indicate much mixing.

Figure 10. Vertical descent profiles of SO_2, O_3, *w'* (the vertical wind component about the mean vertical wind for the profile shown), water vapor mixing ratio (MR), and equivalent potential temperature (θ_e), near 124.5^{o}E 31.1^{o}N for flight 14. Data are 1 Hz except for 10 Hz *w'*. The variances for *w'*, θ_e, and MR indicate that the mixed layer was near 170 m. Note the sharp decreases in SO_2 and CO at 800 m where the turbulence becomes small.

Figure 11. Vertical ascent profiles of SO_2, O_3, *w'* (the vertical wind component about the mean vertical wind for the profile shown), water vapor mixing ratio (MR), and equivalent potential temperature (θ_e), near 124.5^{o}E 30.2^{o}N for flight 14. Data are 1 Hz except for 10 Hz *w'*. At this southern end of the flight track a well developed mixed layer of 600 m has evolved. The SO_2 and

O_3 plume around 1.5 km is in a relatively dry, non-turbulent air parcel that had recently descended from 4 km (see trajectory with circles in figure 12).

Figure 12. Back trajectories for flight 14 from selected points along the 124.5^{o}E flight relating to the vertical profiles of figures 8 to 11: down triangles: 35.7^{o}N 650 m, right point triangles: 35.7^{o}N 1.6 km, star: 34-36^{o}N 150 m, squares: 34.2^{o}N 600 m, up triangles: 31.1°N 400 m, diamonds 30-31^{o}N 150 m, circles: 30.2^{o}N 1.6 km. Largest regions of SO_2 emissions by rank [*Streets et al.*, this issue]: 1- Shandong, 2-Sichuan, 3-Shanxi, 4-Hebei, 5-Henan, 6-Jiangsu, 7-Guizhou, 8-Liaoning, 9-Shaanxi, 10-Guangdong.

Figure 13. SO_2 as a function of the ethyne to CO ratio above and below 2.5 km pressure altitude for flights 13 and 14 along the 124.5°E flight path. The 1 Hz data for SO_2 and CO were integrated over the time period of the ethyne samples.

Figure 14. Time series for the SO_2 observations and the CFOR/STEM-2K1 chemical transport model for flight 13. The solid line is the aircraft flight path. Flight track was along 124.5^{o}E from 0315 to 0805 UTC. Spikes in observed SO_2 at 150 m between 0730 and 0750 UTC were from fresh ship plumes.

Figure 15. Time series for the SO_2 observations and the CFOR/STEM-2K1 chemical transport model for flight 14. The solid line is the aircraft flight path. Flight track was along 124.5^{o}E from 0307 to 0605 UTC.

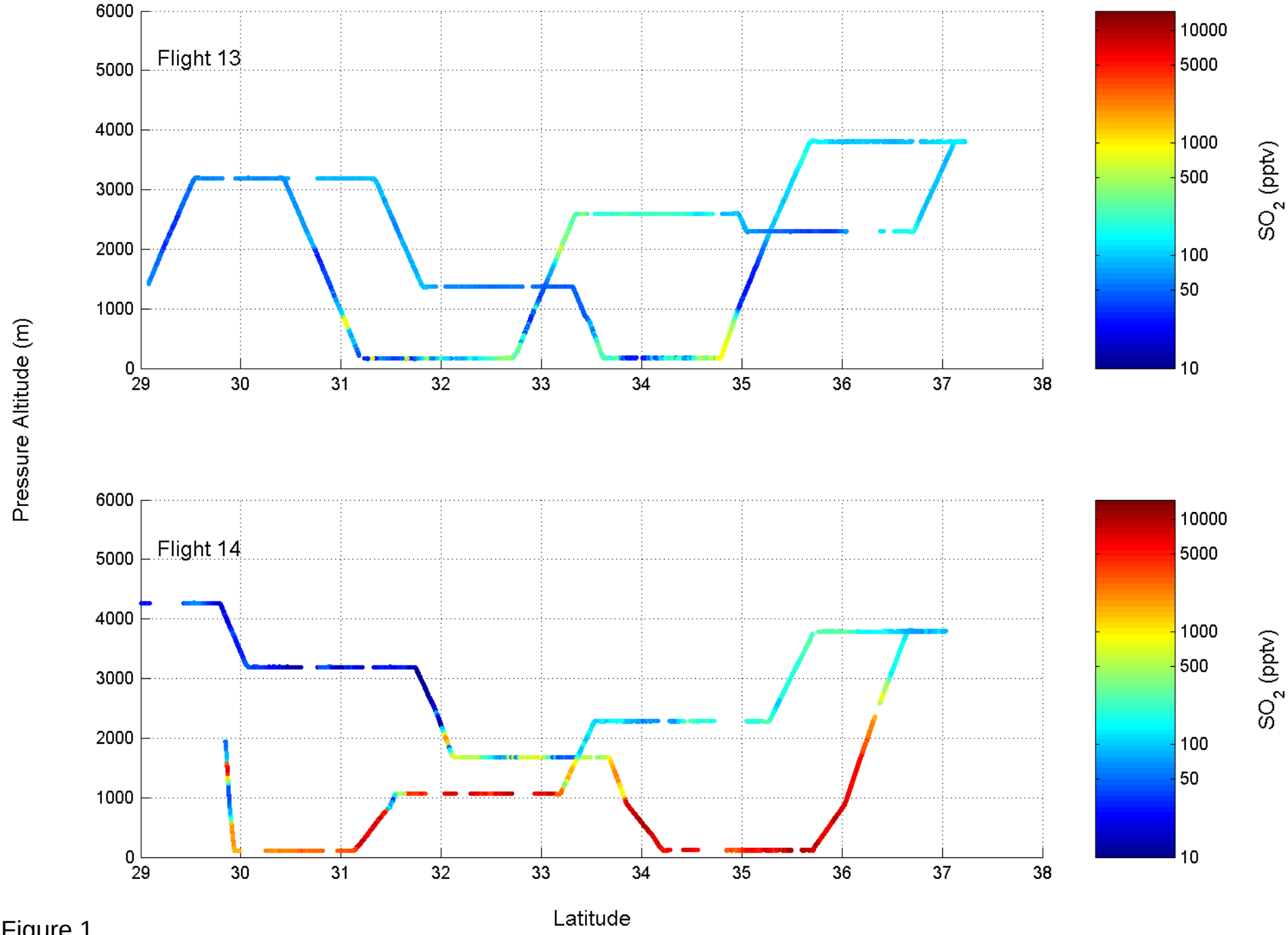
Flight 13
Flight 14
Pressure Altitude (m)
Latitude
SO2 (pptv)
6000
5000
4000
3000
2000
1000
0
29
30
31
32
33
34
35
36
37
38
10000
5000
1000
500
100
50
10

Figure 1

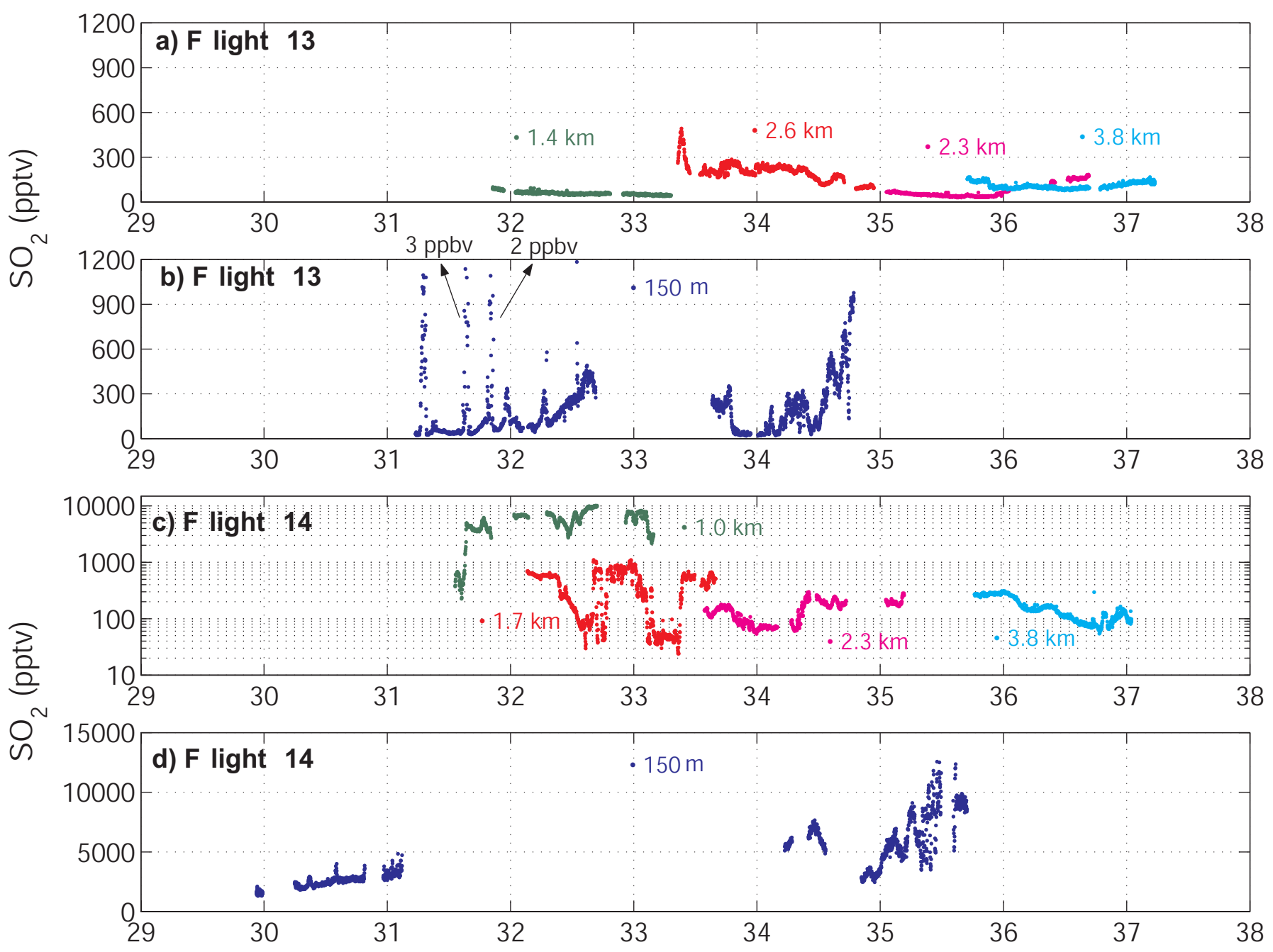
a) F light 13
1.4 km
2.6 km
2.3 km
3.8 km
3 ppbv
2 ppbv
b) F light 13
150 m
c) F light 14
1.0 km
1.7 km
2.3 km
3.8 km
d) F light 14
150 m
SO2 (pptv)
SO2 (pptv)
Latitude

Figure 2

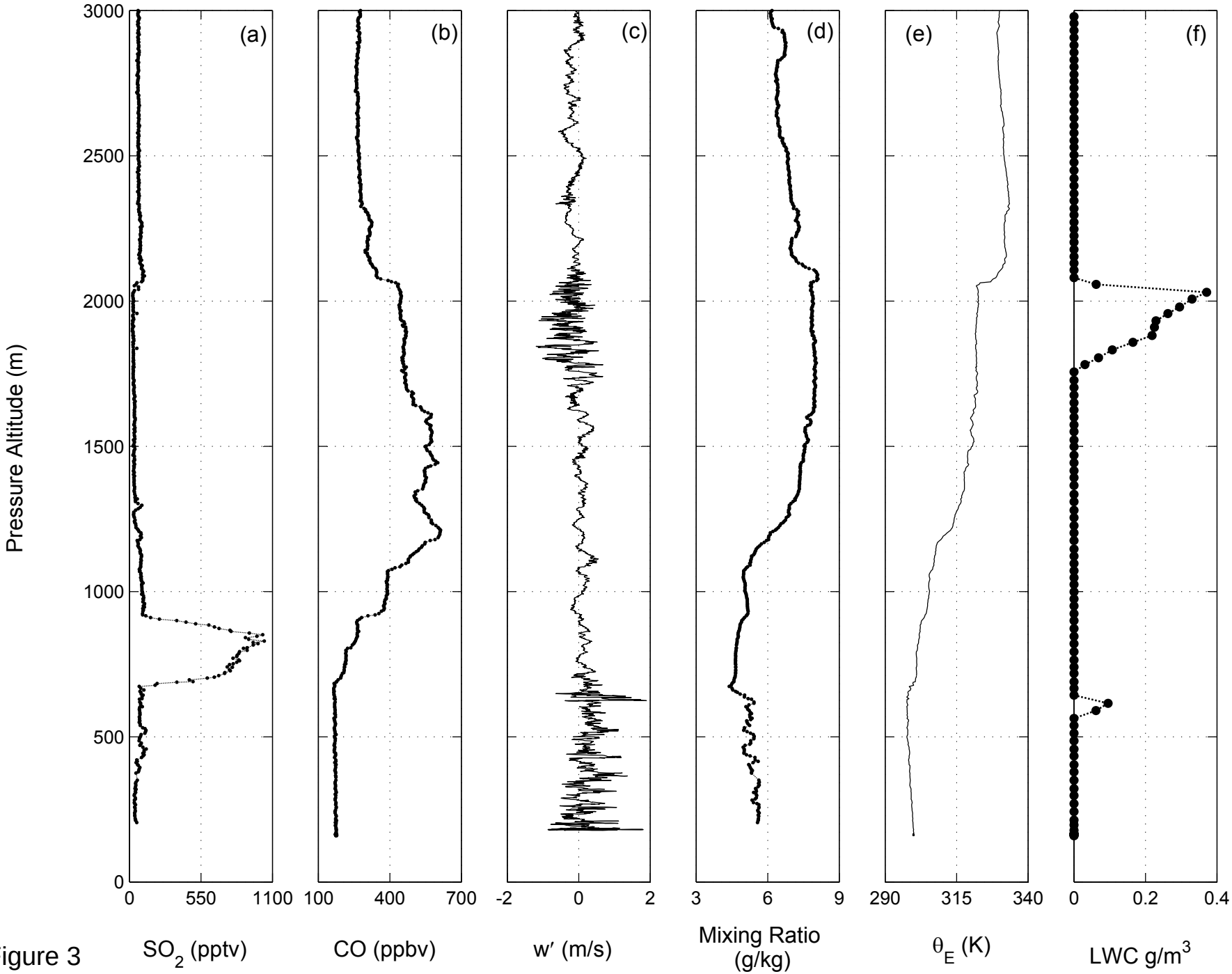
Pressure Altitude (m)
3000
2500
2000
1500
1000
500
0
(a)
(b)
(c)
(d)
(e)
(f)
0
550
1100
100
400
700
-2
0
2
3
6
9
290
315
340
0
0.2
0.4
SO2 (pptv)
CO (ppbv)
w′ (m/s)
Mixing Ratio (g/kg)
θE (K)
LWC g/m3

Figure 3

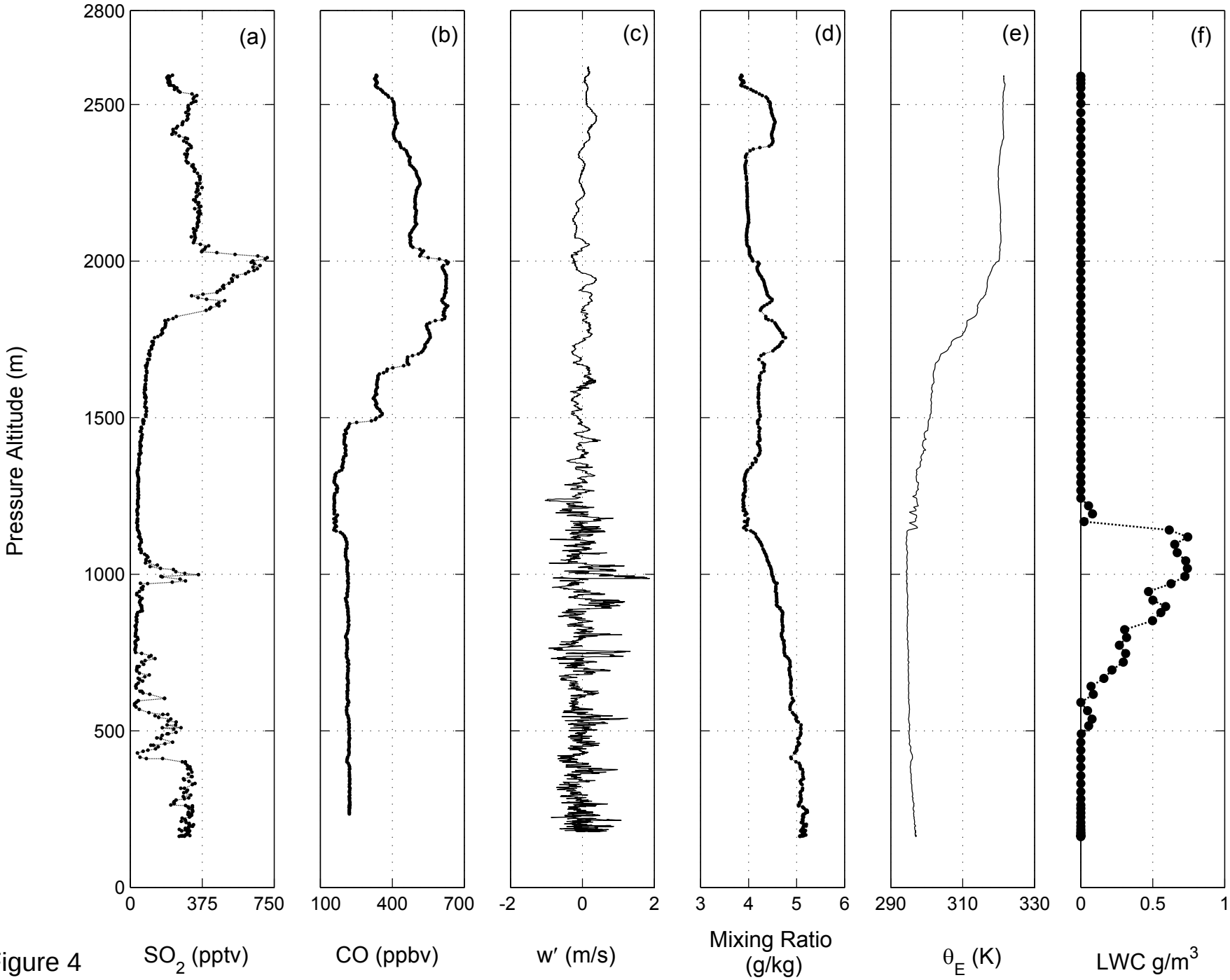
Pressure Altitude (m)
2800
2500
2000
1500
1000
500
0
(a)
(b)
(c)
(d)
(e)
(f)
0
375
750
100
400
700
-2
0
2
3
4
5
6
290
310
330
0
0.5
1
SO2 (pptv)
CO (ppbv)
w′ (m/s)
Mixing Ratio (g/kg)
θE (K)
LWC g/m3

Figure 4

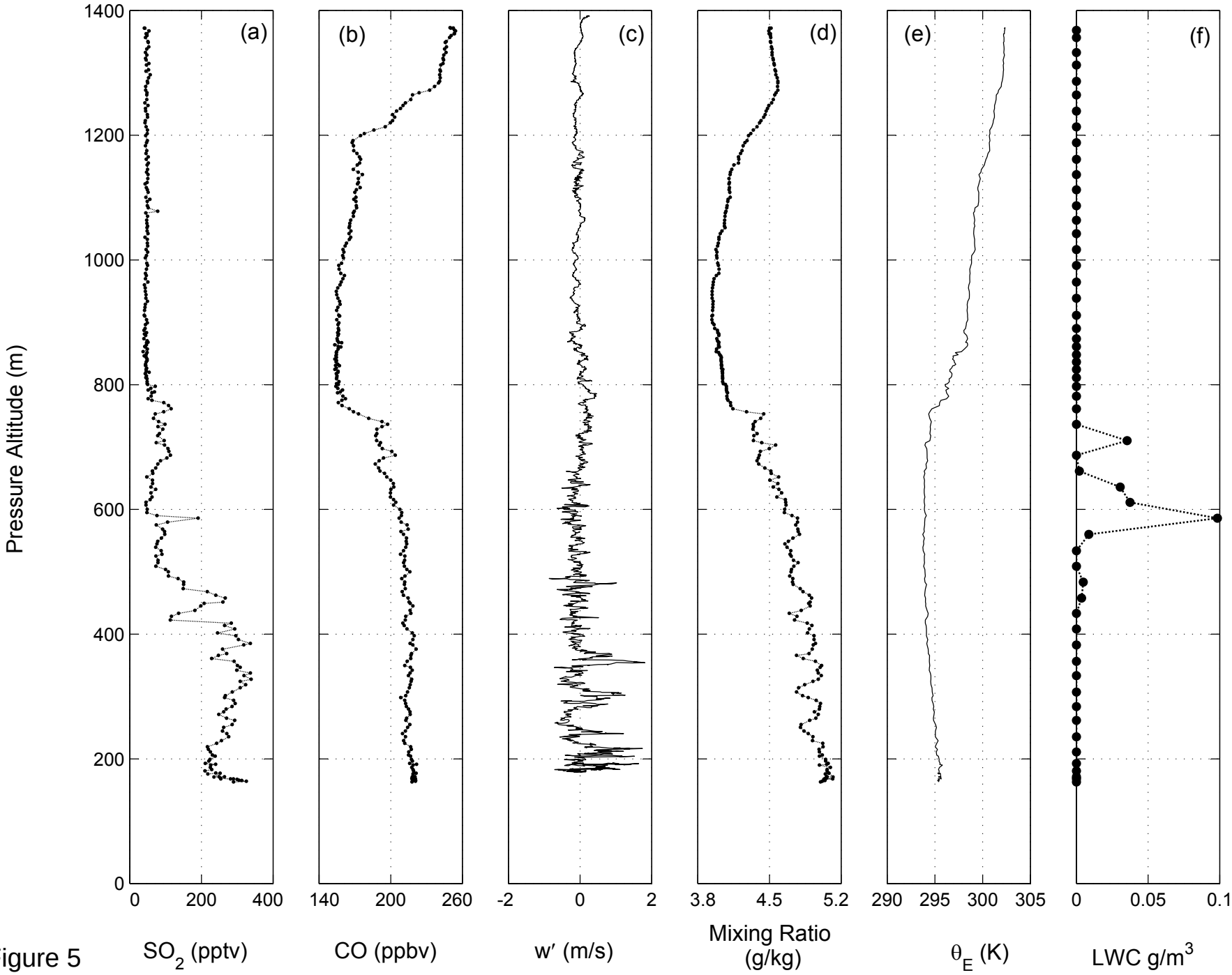
Pressure Altitude (m)
1400
1200
1000
800
600
400
200
0
(a)
(b)
(c)
(d)
(e)
(f)
0
200
400
140
200
260
-2
0
2
3.8
4.5
5.2
290
295
300
305
0
0.05
0.1
SO2 (pptv)
CO (ppbv)
w′ (m/s)
Mixing Ratio (g/kg)
θE (K)
LWC g/m3

Figure 5

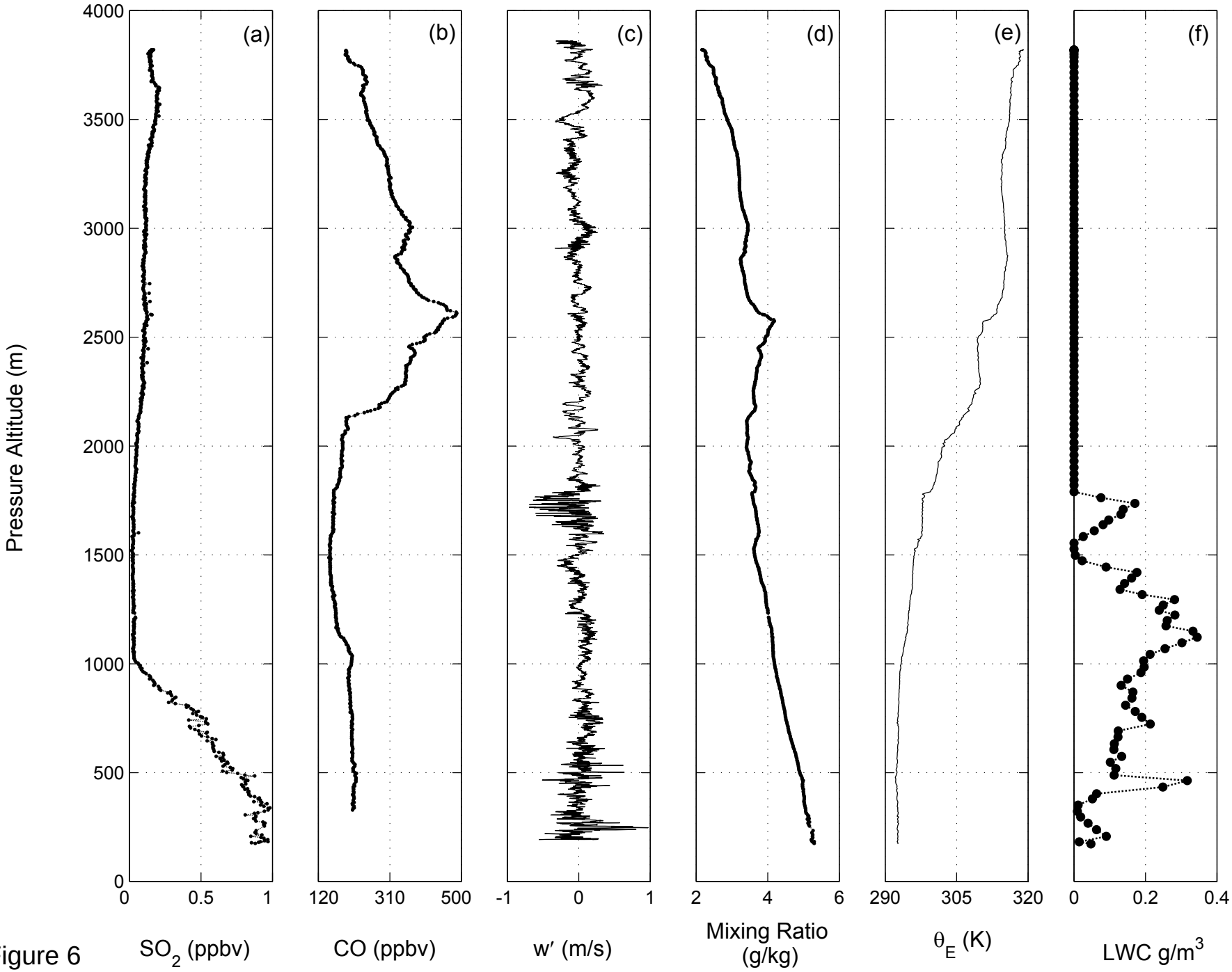
Pressure Altitude (m)
4000
3500
3000
2500
2000
1500
1000
500
0
(a)
0
0.5
1
SO2 (ppbv)
(b)
120
310
500
CO (ppbv)
(c)
-1
0
1
w′ (m/s)
(d)
2
4
6
Mixing Ratio (g/kg)
(e)
290
305
320
θE (K)
(f)
0
0.2
0.4
LWC g/m3

Figure 6

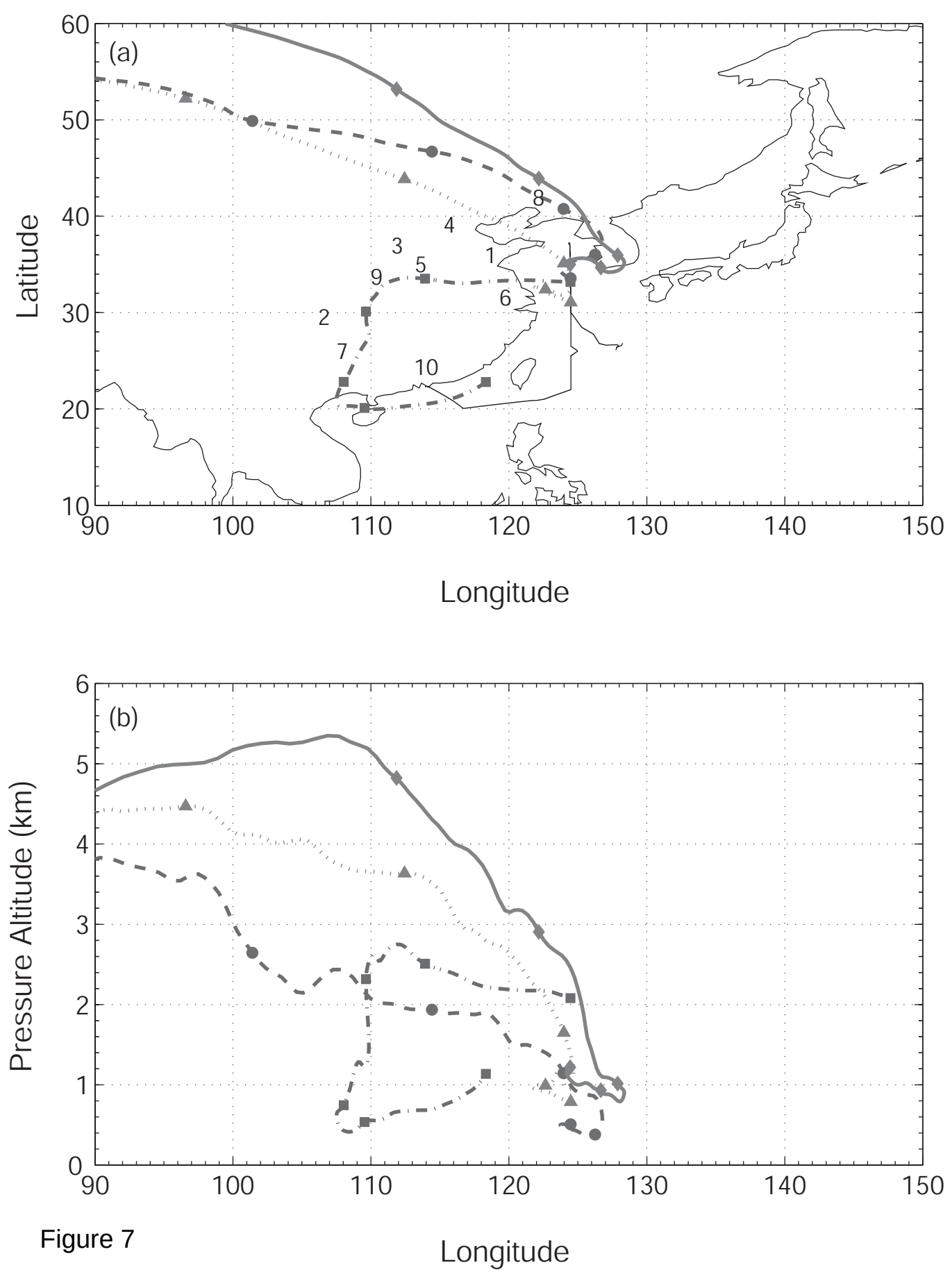
(a)
Latitude
Longitude
60
50
40
30
20
10
90
100
110
120
130
140
150
1
2
3
4
5
6
7
8
9
10
(b)
Pressure Altitude (km)
Longitude
6
5
4
3
2
1
0

Figure 7

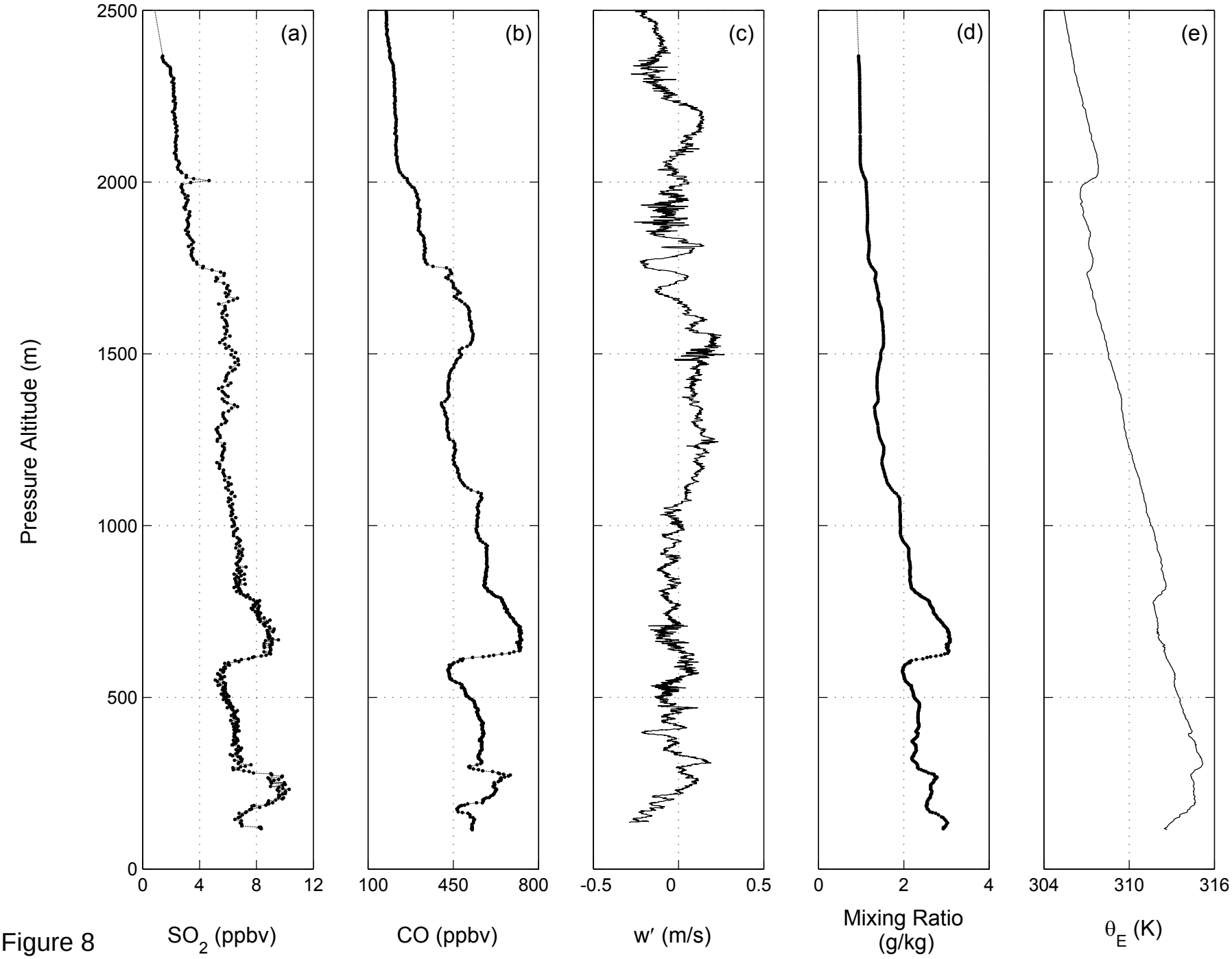
Pressure Altitude (m)
2500
2000
1500
1000
500
0
(a)
0
4
8
12
SO2 (ppbv)
(b)
100
450
800
CO (ppbv)
(c)
-0.5
0
0.5
w′ (m/s)
(d)
0
2
4
Mixing Ratio
(g/kg)
(e)
304
310
316
θE (K)

Figure 8

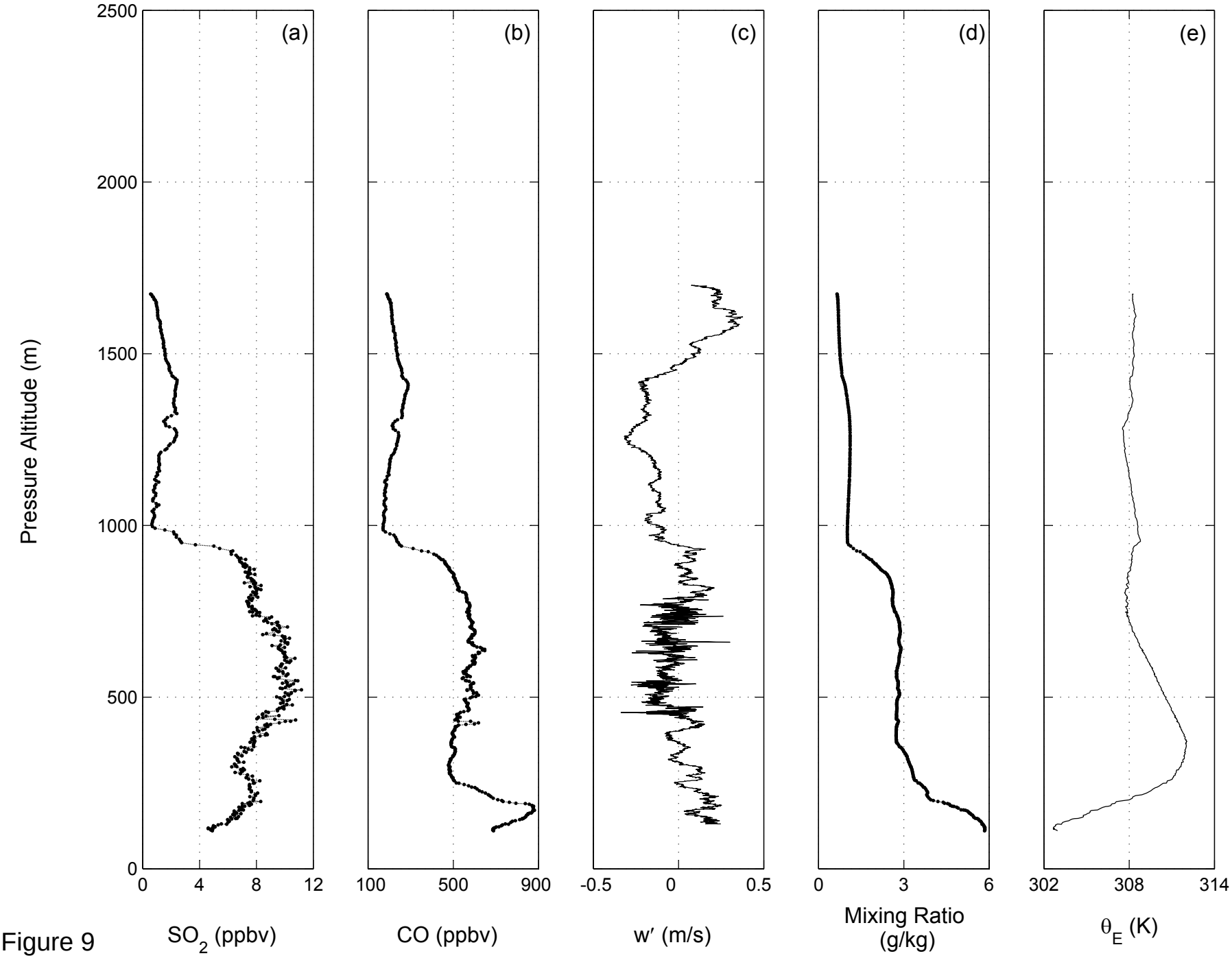
Pressure Altitude (m)
2500
2000
1500
1000
500
0
(a)
(b)
(c)
(d)
(e)
0
4
8
12
100
500
900
-0.5
0
0.5
0
3
6
302
308
314
SO2 (ppbv)
CO (ppbv)
w′ (m/s)
Mixing Ratio (g/kg)
θE (K)

Figure 9

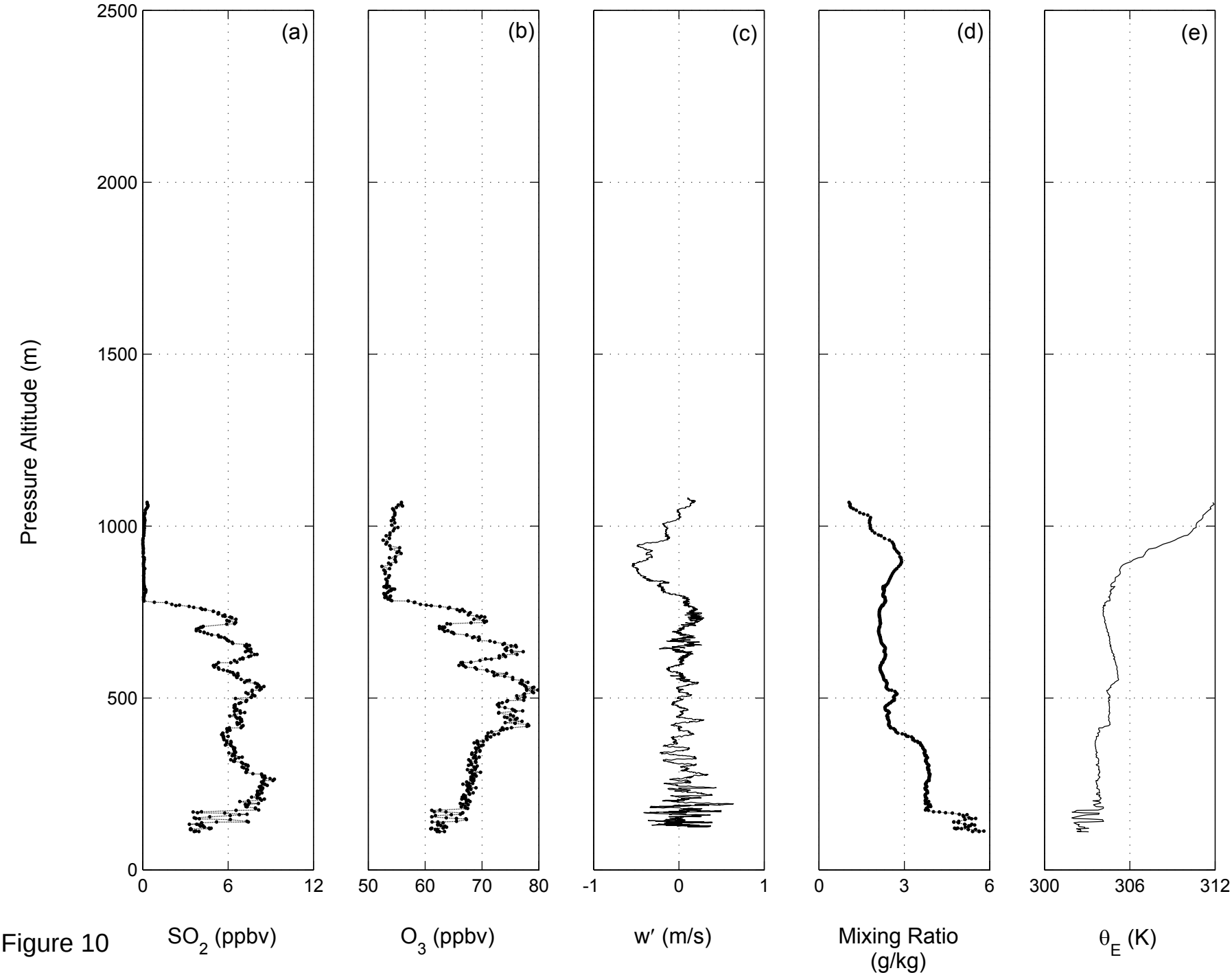
Pressure Altitude (m)
2500
2000
1500
1000
500
0
(a)
(b)
(c)
(d)
(e)
0
6
12
50
60
70
80
-1
0
1
0
3
6
300
306
312
SO2 (ppbv)
O3 (ppbv)
w′ (m/s)
Mixing Ratio
(g/kg)
θE (K)

Figure 10

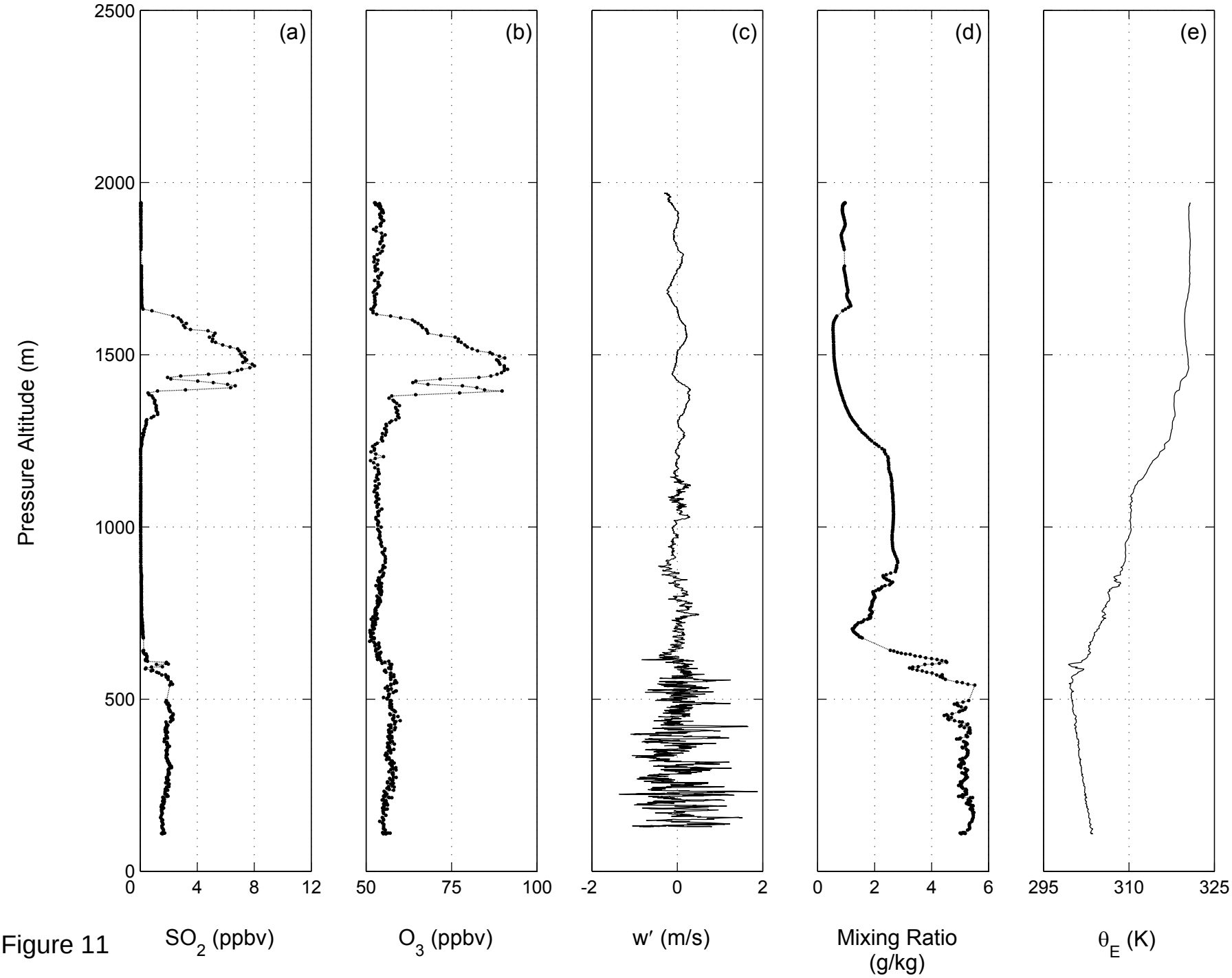
Pressure Altitude (m)
2500
2000
1500
1000
500
0
(a)
(b)
(c)
(d)
(e)
0
4
8
12
50
75
100
-2
0
2
0
2
4
6
295
310
325
SO2 (ppbv)
O3 (ppbv)
w′ (m/s)
Mixing Ratio (g/kg)
θE (K)

Figure 11

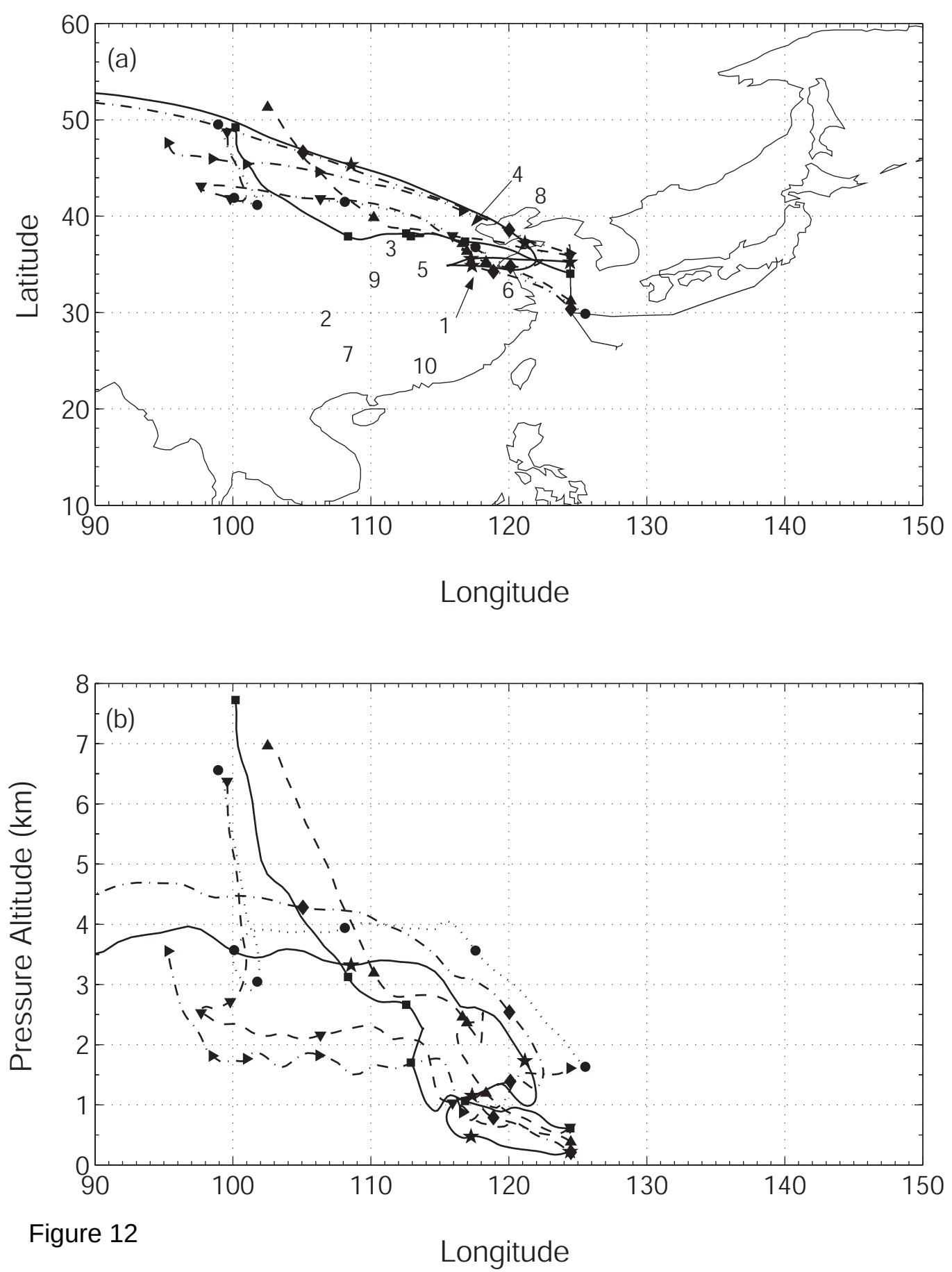
(a)
Latitude
Longitude
60
50
40
30
20
10
90
100
110
120
130
140
150
1
2
3
4
5
6
7
8
9
10
(b)
Pressure Altitude (km)
Longitude
8
7
6
5
4
3
2
1
0

Figure 12

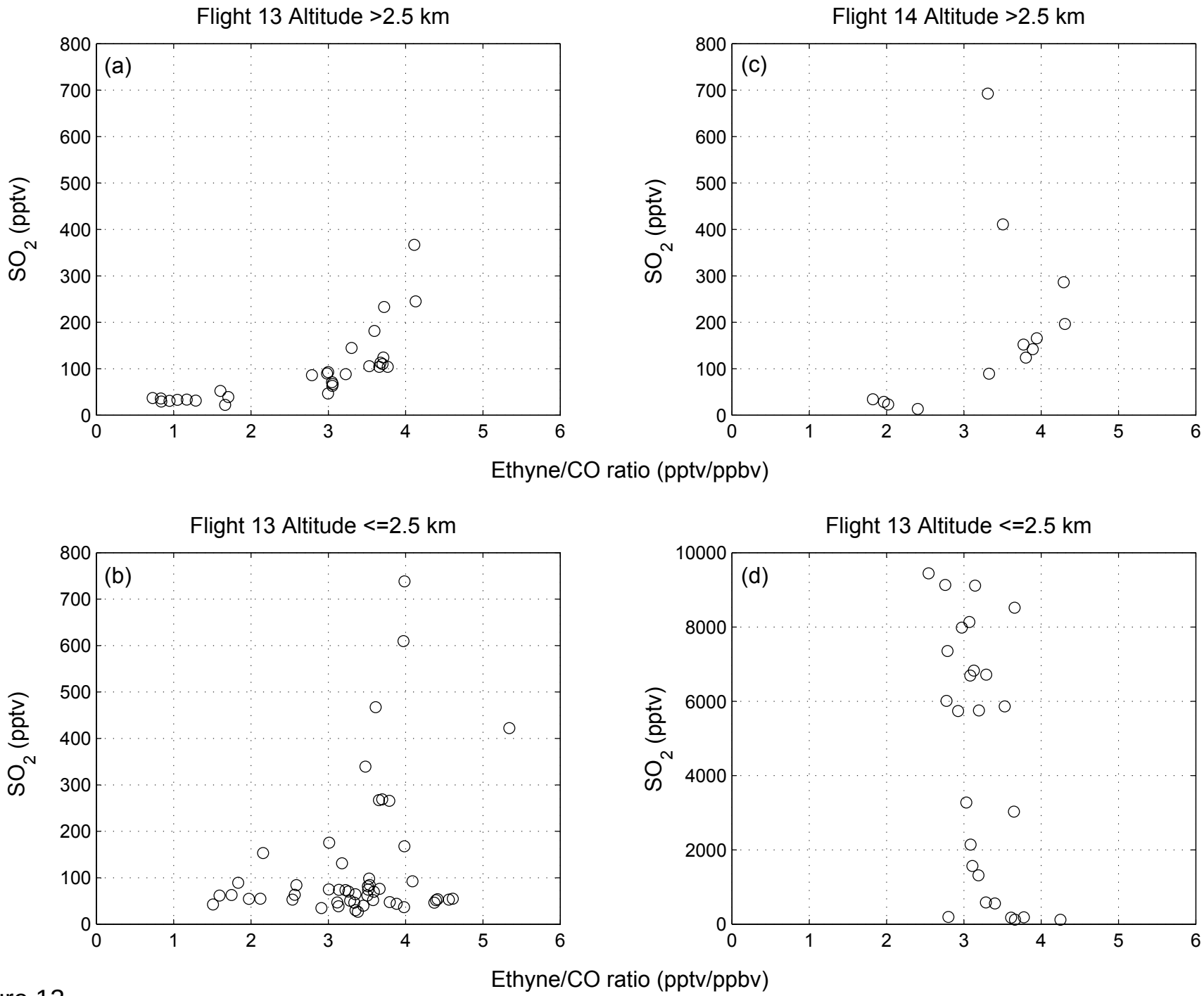
Flight 13 Altitude >2.5 km
(a)
Flight 14 Altitude >2.5 km
(c)
Flight 13 Altitude <=2.5 km
(b)
Flight 13 Altitude <=2.5 km
(d)
SO2 (pptv)
Ethyne/CO ratio (pptv/ppbv)

Figure 13

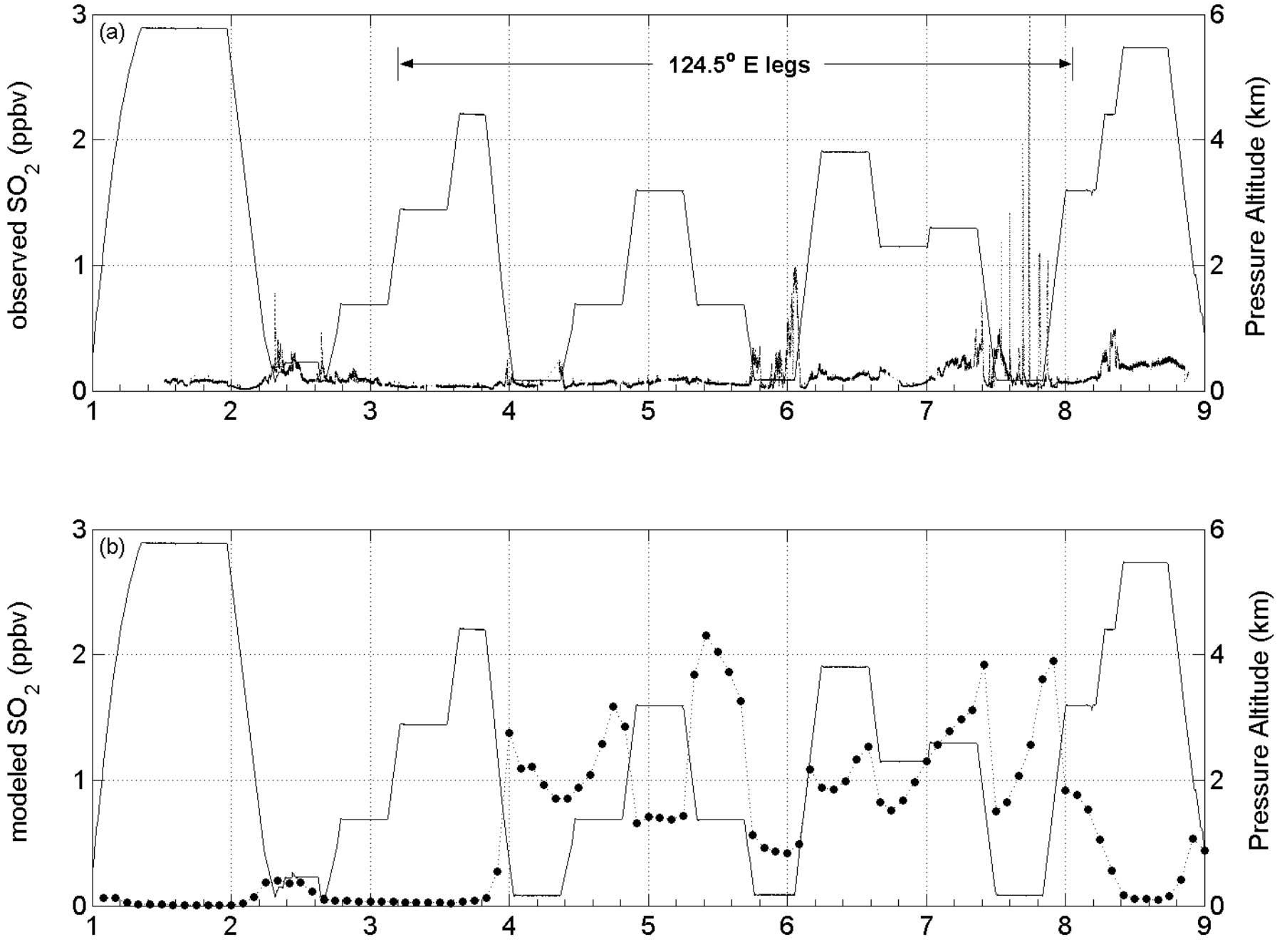
(a)
124.5° E legs
observed SO2 (ppbv)
Pressure Altitude (km)
(b)
modeled SO2 (ppbv)
Pressure Altitude (km)
Flight 13: 17 Mar 01 UTC (hr)

Figure 14

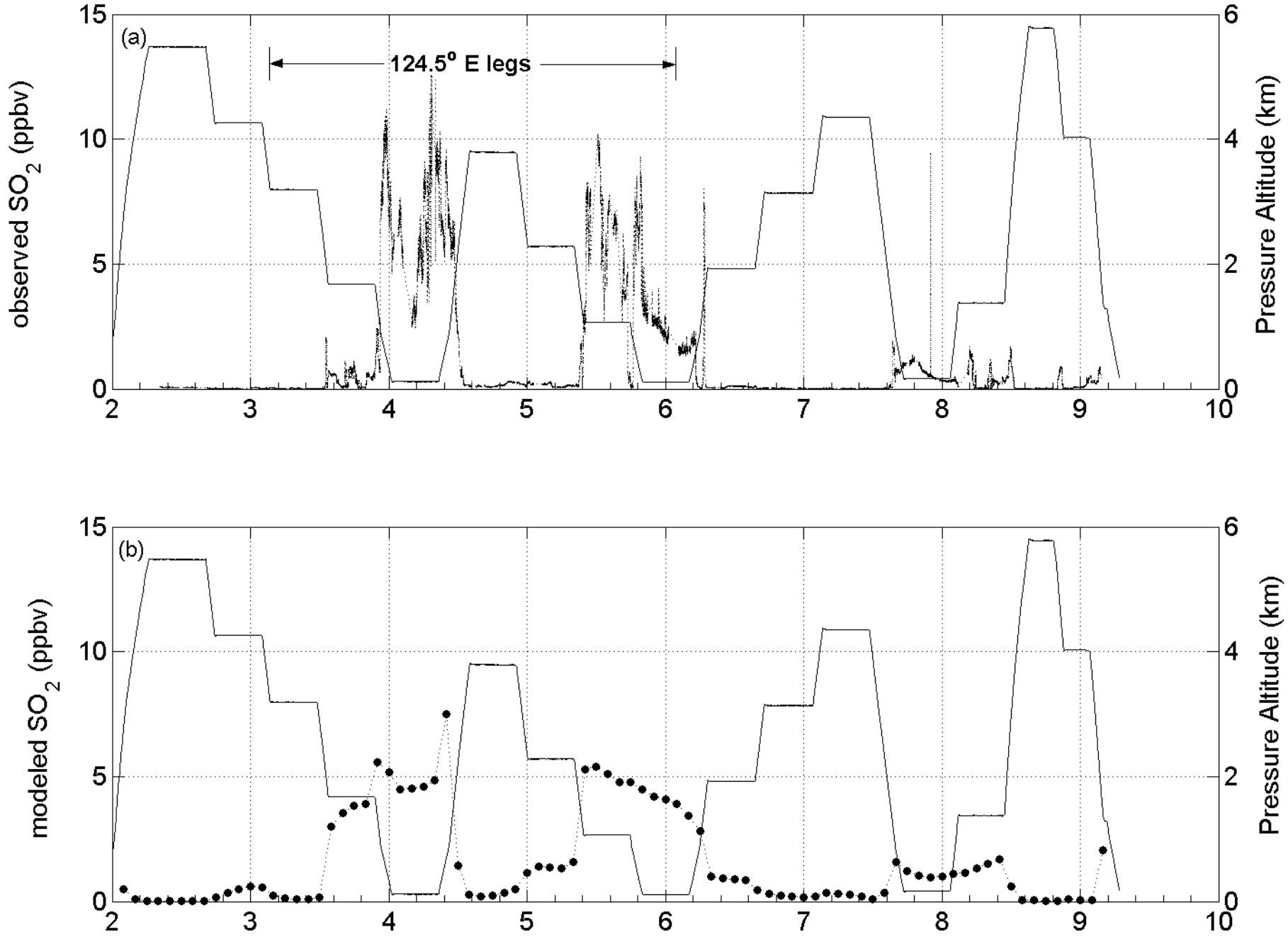
(a)
124.5° E legs
observed SO2 (ppbv)
Pressure Altitude (km)
(b)
modeled SO2 (ppbv)
Pressure Altitude (km)
Flight 14: 18 Mar 01 UTC (hr)

Figure 15